TOWARDS HIGH QUALITY EPITAXIAL $LiNbO_3$ AND $LiTaO_3$ THIN FILMS FOR ACOUSTIC AND OPTICAL APPLICATIONS

Ausrine Bartasyte,[#∃] Samuel Margueron,[+] Thomas Baron,[#] Stefania Oliveri,[#] and Pascal Boulet*

[#]*Femto-ST Institute, University of Bourgogne Franche-Comté, CNRS UMR 6174, 15B Avenue des Montboucons, Besançon, F-25030, France*

[+] *Laboratoire Matériaux Optiques, Photoniques et Systèmes, Université de Lorraine et Centrale Supelec, EA 4423, 2 rue Eduard Belin, Metz, F-57070, France*

* *Institute Jean Lamour, CNRS (UMR 7198) – Université de Lorraine, Parc de Saurupt, F-54011 Nancy, France*

[∃] *ausrine.bartasyte@femto-st.fr*

ABSTRACT

Over the past five decades, $LiNbO_3$ and $LiTaO_3$ single crystals and thin films have been studied intensively for their exceptional acoustic, electro-optical, pyroelectric and ferroelectric properties. Today, $LiNbO_3$ single crystals in electro-optics are equivalent to silicon in electronics and about 70 % of rf filters, based on surface acoustic waves, are fabricated on these single crystals. These materials in the form of thin films are needed urgently for the development of the next generation of high–frequency and/or wide-band RF filters or tuneable frequency filters adapted to the 5th generation of infrastructures/ networks/ communications. The integration of $LiNbO_3$ films in guided nanophotonic devices would allow higher operational frequencies, wider bandwidth and miniaturized optical devices in line with improved electronic conversion. Here, the challenges and the achievements in the epitaxial growth of $LiTaO_3$ and $LiNbO_3$ thin films and their integration with silicon technology and to acoustic and guided nanophotonic devices are discussed in detail. The systematic representation and classification of all epitaxial relationships reported in the literature have been carried out in order to help the prediction of the epitaxial orientations in the new heterostructures. Future prospects of potential applications and the expected performances of thin film devices are overviewed, as well.

Ausrine Bartasyte is an associate professor – chair of excellence of Labex ACTION at the Institute FEMTO-ST, University of Bourgogne Franche-Comté (Besançon, France). She received her Ph.D. in 2007 from Grenoble Institute of Technology. She was a postdoctoral research assistant in Prof. A.M. Glazer's group at the University of Oxford, Oxford, UK, working on the crystal growth of $LiNbO_3 - LiTaO_3$ solid solutions. Her research interests include metal–organic CVD, thin films and crystals of alkaline niobates and their applications in acoustics and optics.

Samuel Margueron is an associate professor in physics at the Laboratoire Matériaux Optiques, Photonique et Système, of the University of Lorraine and CentraleSupelec. He received his Ph.D. in 2003 from the Office National d'Etude et de Recherches Aérospatiale (ONERA), then he was a post-doctoral research assistant in D.R. Clarke's group at the UC Santa Barbara. His research activities concern the spectroscopy of micromechanical properties of integrated functional oxides, ferroelectrics and semiconductors.

Thomas Baron is a research engineer at Institute FEMTO-ST/ENSMM (Besançon, France). He obtained his PhD in Nano and Micro Electronics from the University Joseph Fourier in Grenoble in 2008. His Ph.D. was focused on the integration of NEMS with the industrial CMOS process based on SOI technology. His current research is focused on micro fabrication processes, including layer transfer techniques, of acoustic filters and resonators based on single crystalline materials and thin films.

1. INTRODUCTION

1.1. $LiNbO_3$ AND $LiTaO_3$ SINGLE CRYSTALS

In 1928 Zachariasen discovered the $LiNbO_3$ phase.[1] The first single crystals were grown using the flux method by Remeika and Matthias in 1949.[2] The possibility of growing single crystals with large dimensions using the Czochralski technique was demonstrated by Ballman in 1965, this initiated intense study of the physical and structural properties of these crystals.[3] The ilmenite structure of $LiNbO_3$ (LN) and $LiTaO_3$ (LT) crystals have been resolved by Abrahams et al.[4,5] LN and LT are isostructural ferroelectric materials and belong to R3c space group at room temperature (**Figure 1**), but have different physical and structural properties. LN presents a much higher Curie temperature ,T_c, (around 1050°C)[6] than LT (around 600°C).[7] LT melts about 400°C higher than LN.[8,9] The solid solutions LN-LT are of particular interest due to the possibility of tuning the physical properties of LN in a controlled way to those of LT and vice versa.[10-12] LN and LT phases exist over a wide compositional range (from 46.5 to 50.5 mol% of Li_2O).[8,9] Outside this range two phases coexist: $LiNb(Ta)_3O_8$ and $Li_{0.93}Nb_{1.07}(Ta)O_{3.14}$ at 25 < Li_2O mol% < 46.5 and $Li_3Nb(Ta)O_4$ and $LiNb(Ta)O_3$ at 50.5 < Li mol% < 75. The congruent compositions of LN and LT are nonstoichiometric (48.38 mol% and 48.39 mol% of Li_2O, respectively).[6,7] The physical and structural properties of LN and LT are highly dependent on the Li non-stoichiometry. For example, the Curie temperatures of congruent and (nearly) stoichiometric LT (LN) are 605°C (1141°C)[6,7] and 701°C (1198°C), respectively.[8,13] The coercive field in congruent LT crystals is 211 kV/cm while it is only 1.4 kV/cm in stoichiometric ones.[14] Elastic constants,[15] density,[16,17] electromechanical coupling (K^2),[18] acoustic velocity,[18,19] refractive indices,[20] birefringence,[8] UV absorption edge,[21] and photorefractive damage[22] are also highly dependent on the deficiency in Li. Therefore, the composition of the crystals has to be precisely controlled for large-scale device production. Lithium is a light element and its concentration within the crystals can be estimated only by destructive direct methods (chromatography,[23] atomic absorption analysis,[16] or inductively coupled plasma atomic emission spectroscopy (ICP-AEA),[24] which may require a large amount of material and can offer a precision no better than 0.2 mol%. To overcome these limitations numerous indirect non-destructive methods of compositional analysis, based on the calibration of the relationships between Li non-stoichiometry and the physical and structural properties, have been developed. Wohlecke et al. have reviewed these relationships and the precision and accuracy of the indirect methods which were used for the analysis of Li content in LN crystals.[25] A precision of 0.01-0.05 mol% and accuracy of 0.1 mol% can be attained by indirect methods based on measurements of birefringence, UV absorption edge and Raman mode damping. Birefringence imaging and Raman spectroscopy can be used to map the homogeneity of the crystal composition.[26] The Curie temperature, T_c, is a widely accepted method of determining the composition of LT crystals. As mentioned above the stoichiometric composition of LN/LT is not congruent. Thus, the growth of homogeneous stoichiometric crystals is challenging and was achieved by a double crucible Czochralski method or by post-growth treatment of the congruent wafer by vapour transport equilibration in a Li_2O rich atmosphere. So far, the stoichiometric LN and LT crystals are relatively expensive and their availability is very limited. At present the best control of the LN/LT crystal composition has been attained by growing the crystals with congruent composition by the Czochralski technique. Congruent LN and LT single crystals with diameters up to 150 mm, grown by the Czochralski method, are produced industrially. The congruent crystals have high electromechanical coupling, pyroelectric and electro-optic coefficients thus, they are widely used in acoustic, pyroelectric and electro-optical devices, described in more detail in the following sections.

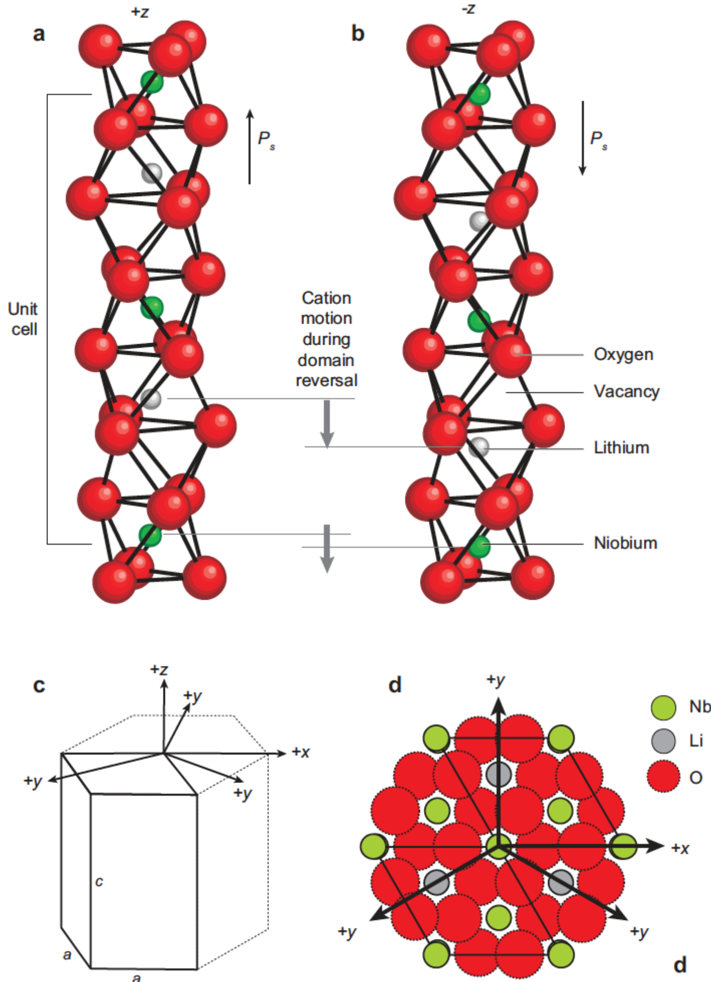

Figure 1. (a) (b) The crystal structure of ferroelectric $LiNbO_3$ and $LiTaO_3$ (space group R3c). The cation displacements with respect to the oxygen network in Z+ and Z- domains. (c) The relationship between hexagonal settings used to describe the rhombohedral structure and orthogonal settings (XYZ), applied in the description of the physical properties. (d) A schematic view of the hexagonal unit cell along the c-axis. Reproduced with permission. [14] Copyright 2007, Annual reviews.

Note that the conventional labelling of the LN and LT crystal cuts in the hexagonal settings (axis and planes), orthogonal XYZ settings (used for the tensor description of the physical properties), IEEE convention[27] and Euler angles is as shown in **Table 1**.

1.2. GUIDED PHOTONICS

Advances in optical-fibre-based communications have revolutionized the internet over the past 30 years. The first LN and LT waveguides were formed by out-diffusion of Li_2O so that the extraordinary index of refraction increased at the surface.[28] Optical waveguides were also formed in crystals by in-diffusion of transition metal ions,[29,30] by liquid phase epitaxial growth (LPE),[31,32] by the implantation of various ions,[33-35] by annealed proton exchange (APE),[36,37] or reverse proton exchange (RPE).[38-40] Since then many different devices have been fabricated in the form of integrated waveguides in the laboratory and were applied in industry for telecom and sensor applications: amplitude modulator, phase modulator, polarization modulator, rotating waveguide, Bragg deflector modulator, Fabry-Perot resonator, interferometric modulator such as Mach-Zehnder-type interferometer, electro-optic shifter and compressor, mode locked laser beam switch, switched directional couplers, second harmonic generator in a periodically poled waveguide, integrated parametric oscillator and converter, etc.[41,42]

The development of integrated waveguides has been facilitated by microelectronic technology such as photo- and electron-lithographies which allowed the fabrication of sophisticated optical and electronic devices. However, LN and LT are very inert materials, many efforts have been made to develop two and three dimensional structures: ridges, waveguides, periodic photonic crystals, microwires, micro-disks or nanostructures. Different techniques were used for this purpose: differential HF etching of Z+ and Z- faces,[43] plasma etching,[44,45] focussed ion beam (FIB),[46] saw dicing, polishing and lapping,[47] femtosecond laser cutting or writing. To improve the efficiency, combinatorial techniques such as differential HF etching of Z+ and Z- faces under ultraviolet illumination,[48] combination of proton exchange and plasma etching,[49] or a combination of ion implantation and etching.[50] Now a new generation of devices is emerging using thin crystals.[51,52] The single-crystal films are fabricated by means of wafer bonding and polishing or by ion-implantation, wafer bonding to the host substrate and slicing during annealing (**Figure 2**).[53,54] The examples of the micro-resonator and CMOS compatible modulator, fabricated by these layer transfer techniques are given in **Figure 2** and **3**, respectively. The integration of the optical waveguides allowed a significant improvement of electro-optic device performance:

1- The number of modes can be precisely adapted, knowing the thickness and index profile, which limits the modal dispersion effects.[28,55-57]
2- The power per bandwidth ($P/\Delta f$) is proportional to the cross-section divided by the length which is limited by diffraction in the bulk crystal. For waveguides the section is only limited by the electrode spacing.[58] At present the width of commercial waveguide strips is 3-8 μm for Ti in-diffusion and the travelling wave modulator has a power per bandwidth of 60 μW/MHz.
3- Lower power can be used to drive the process. The effective electric field in the waveguide is described by $E = uV/b$, where u is a geometrical factor, V - the applied voltage, and b - the electrode spacing. The modulation of the phase index by the electro-optic effect, normalized by the applied field, depends only on the length of the guide (assuming an electro-optic coefficient similar to that of the bulk LN).[58]
4- The design of the travelling wave modulator as a ridge in a coplanar geometry increases the bandwidth significantly and the response becomes independent of the capacitance and the load resistance of the circuit. The only limitations are dielectric and electrode losses.[59]
5- Non-linear optical frequency doubling in bulk materials is limited by diffraction and is constrained to small interaction volumes. The use of a waveguide can extend the interaction length and the wavelength range for phase-matched frequency doubling.[60,61]

There are several drawbacks in devices based on waveguides:

1- The profiles created by in-diffusion, proton exchange or ion implantation present inhomogeneous concentration profiles (gradients) and may lead to a transition to non-guiding phases. The lattice changes introduce a complex profile of the refractive index due to the photo-elastic effect and complex electro-optic properties.[40]
2- A SiO_2 buffer layer, currently used for impedance matching, causes DC drift and thermal drift. At high frequency, radiation loss and velocity mismatch cause severe limitations.[62]
3- Mechanical machining, etching, smart-cut and the FIB processing induce surface roughness and point defects which generate surface losses at high frequencies. The FIB cut frequently used for the microfabrication of 3D structures in research laboratories is time consuming and has limited possibilities of being scaling up. The development of cheap and precise methods that are transferable to large-scale micro-structuring methods are being investigated by many research groups.

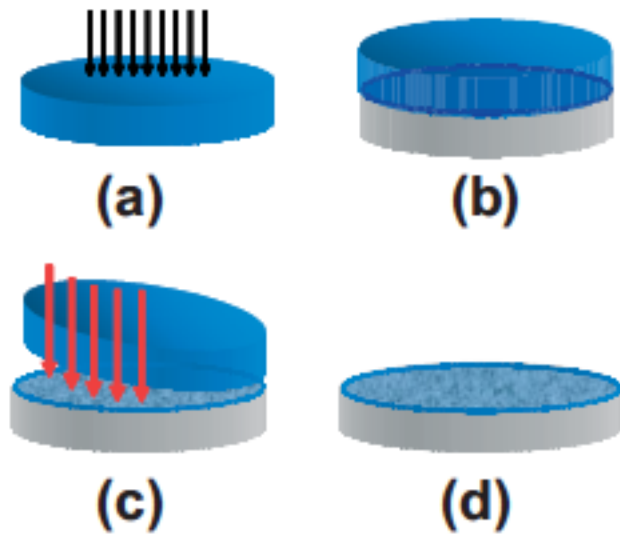

Figure 2. Schematic representation of the layer transfer process by the ion slicing technique consisting of ion implantation (a), wafer bonding (b), laser irradiation or heating in order to obtain a single crystalline layer on the host (Si) substrate (d).
Reproduced with permission. [53] Copyright 2006, WILEY-VCH Verlag GmbH & Co.

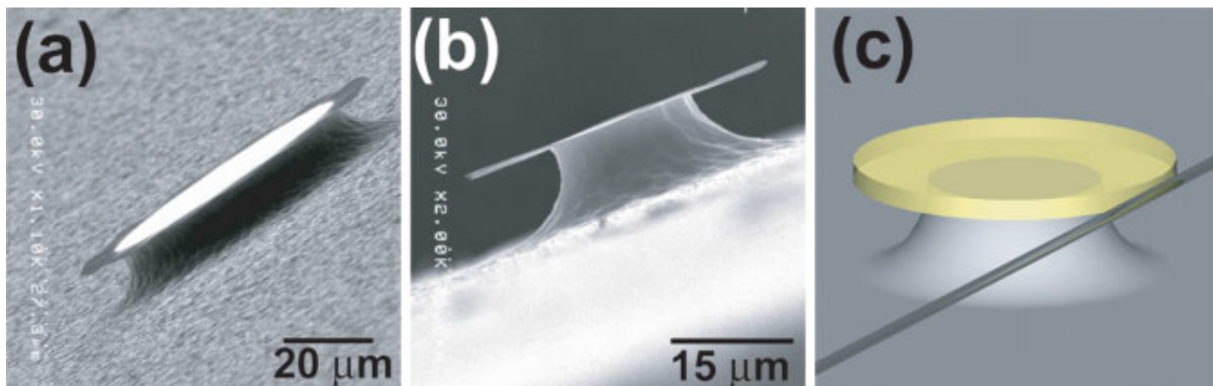

Figure 3. Electron microscopy images (a, b) and schematic diagram (c) of a micro-resonator based on $LiNbO_3$ film on Si and fabricated by the layer transfer technique.
Reproduced with permission. [53] Copyright 2006, WILEY-VCH Verlag GmbH & Co.

The integration of LN layers with the waveguides would allow the attainment of a sharp-change and high-contrast of the refractive index at the substrate to film interface (Δn up to about 0.7). The guiding layer thickness can be adjusted easily by changing the film thickness. High confinement can be attained in the structures based on thin films and these structures can be used for high-density integrated optics. To reach higher operational frequencies, wider bandwidth and miniaturized optical devices, improved electronic conversion is necessary. It is widely held that guided nanophotonics may make this possible. It would require the use of functional oxides with high conductivity however. The modulator, based on a single-crystal LN film on Si, able to operate from DC to 110 GHz has been demonstrated (**Figure 4**).[63] The ability to fabricate compact, all-optical devices such as routers, processors and computers with these functional oxides are new challenges to overcome. Several designs of all-optical devices have been proposed to combine opto-electronic properties of dielectrics for waveguiding, logic operation gates or optical memories. At present, this technology is at a research stage and

designs proposed for all-optical devices are too expensive for industrial fabrication and manufacturing of three dimensional structures induces high losses in light propagation.

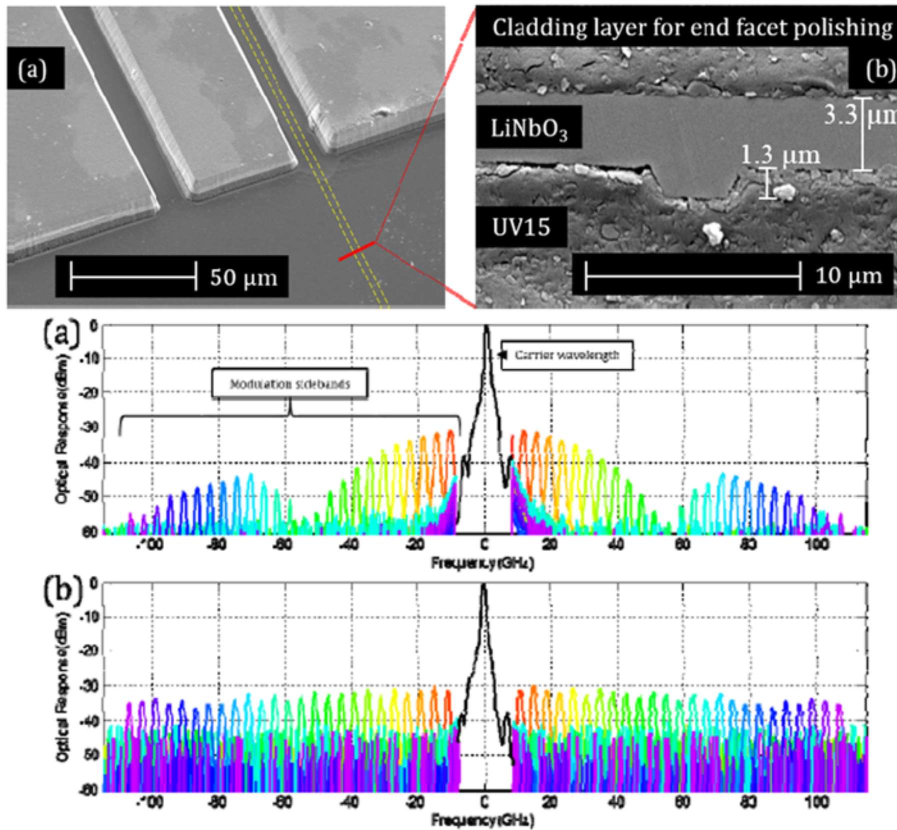

Figure 4. A 110 GHz CMOS compatible modulator based on $LiNbO_3$ thin film on silicon: top and cross sectional views of the inverted ridge waveguide (a and b, top), optical frequency response of a carrier modulated with RF with up to 110 GHz in untuned (a, bottom) and tuned (b, bottom) devices. Reproduced with permission. [63] Copyright 2016, OSA.

1.3. RF ACOUSTIC FILTER APPLICATIONS

Radio frequency (RF) filters are used in the fields of information and communication (mobile phones, data analysis, Wi-Fi, DSL), automotive navigation/toll systems, medical instruments, industry, household appliances, military applications, etc. The market of RF filters is over 4.3 billion euros. Communication, information and control systems offer progressively more functionalities in line with miniaturization of electronic components. This requires more RF bands and more complex RF circuits without increasing the total size or the total energy consumption of the systems. Miniaturization concerns the integration of passive devices which are often discrete parts and occupy ~60% of the total area of handheld devices.[64] Surface acoustic wave (SAW) devices such as filters, resonators, duplexers, requiring specific materials (such as LN or LT) unavailable in the form of thin films, are placed outside the chip package introducing inefficient connections and parasitic inductances. Despite the extreme reduction of discrete filter size (by 85%), the minimum size of filters is still around 0.3 - 0.5 mm^2. With the increasing use of wireless electronics it has become essential to produce miniaturized, reliable, and low cost systems with high performance.

Mobile telecommunication (which requires compact space usage) relies on RF filters made of piezoelectric materials. They excel by virtue of the low losses at high frequencies, i.e. the 1-10 GHz range. Generally, such piezoelectric RF filters can be based on surface acoustic wave (SAW) on single crystal piezoelectric materials (mainly LN or LT single-crystal wafers), or recently thin film bulk acoustic wave resonators (TFBARs) exploiting thickness mode resonances in a thin AlN piezoelectric film.[65,66] To be applied, RF filters must have very low insertion losses (< 2 dB at 2

GHz), low frequency drift with temperature, a relative band-pass of 3-10% with respect to the central frequency, and a pure spectral signature. Conventional RF filters based on SAW can reach frequencies up to 3.5 GHz. The demand of SAW filters increased enormously when smartphones came to the market. RF filters are used for S and C bands in space and military applications, as well. Military and space applications represent a much smaller market but demand extreme performance. Finally, electrical excitation of acoustic waves is also used in wireless sensors, which is a very innovative and fast-growing field.

So far, SAW and BAW (bulk acoustic wave) technologies are complementary, but SAW RF filters are less expensive than BAW, the latter being mostly used for high performance RF filters with high power handling capabilities. Further increases in the frequency of conventional RF SAW filters is limited by the period of interdigitated electrodes (limit of deep UV lithography), but the main restrictions are the phase velocity or electromechanical coupling coefficient, K^2, of available materials. Thus, they cannot be used for filters operating at high frequencies (> 3.5 GHz). SAW filters suffer from poor stability at high power densities. Mobile phones today use RF SAW filters with pass band of 3% are used and are fabricated from Y42°LT wafers and h/λ=8% Al electrodes (where h is a film thickness and λ – the wavelength). So far there are few prospects of improving this technology which is based on single-crystals.

Compared to SAW filters, TFBAR filters (market of $300M), based on sputtered AlN films on electrode/Si, are more expensive but can provide lower insertion loss, improved selectivity, higher power handling, higher operation frequency (defined by propagation velocity and film thickness), and better electrostatic discharge protection, while offering key advantages for some specific filters (e.g. duplex filters around 1.9 GHz). AlN films offer high quality factors but are limited by their low K^2 (7.5%). This electromechanical coupling factor is sufficient to synthesize filters in the 2-3 GHz range, but as the frequency increases the thickness of the piezoelectric film needs to be decreased, while the thickness of other layers stays almost the same. This decreases the effective electromechanical coupling factor of resonators and the bandwidth. Hence, it is generally agreed that the upper frequency limit for BAW resonators is close to 4 GHz, which limits the widespread use of this technology.[67,68] New suitable low loss materials are needed with larger K^2 to achieve larger bandwidth: this is essential for wireless telecommunication in which the amount of data transmitted is rapidly increasing. It is also important for the satellite industry, which requires filters in the 2-6 GHz range. Evolution of communication systems and continuously increasing transmission of information through different channels (4G) require on one hand increasing the number of bands (up to 8) assigned for transmission of data (dynamic images, sound, internet, data base…) and on the other hand increasing the width of the band pass and/or the working frequency in order to improve the transmission of data. This requires more RF bands and more complex RF circuits without increasing the total size of the systems. There are about 50 filters in a smartphone, by 2020 the number of filters will have to increase to 100. Therefore, another emerging research topic is the ability to make tuneable frequency filters that would enable reconfigurable RF front-ends which would radicallly reduce the number of components.[68] In this case, filters need to continue satisfying existing specifications while providing new functionalities. These applications require resonators with large K^2, requiring in turn highly piezoelectric materials. New materials are needed for thin film piezoelectric resonators intended for frequency control elements, an upcoming application where improved piezoelectric properties would be useful for integrated oscillators.[69] Moreover, new materials are needed to allow strong electro-mechanical coupling and compatibility to photonic devices, which is highly relevant to devices that couple wireless to optical fibre networks.

To summarize, modern communication systems, device miniaturization and integration require the ultra-wide band and high-frequency or tuneable frequency RF filters while maintaining and improving other important properties such as the quality factor, the electromechanical coupling (directly related to the bandwidth and thermal stability) and power handling capability. This stimulates further development of SAW and BAW devices.

The frequency of a filter or SAW resonator can be described by $f = v_{\phi}/2p$, where f is the synchronous frequency, p – the period of interdigitated transducers (IDT) and v_{ϕ} – the phase velocity. In the case of single-crystal wafers, there are two ways to increase the frequency of a

filter or resonator: (i) use a material with a high phase velocity; (ii) reduce the period of IDTs. However the phase velocity in single crystals is limited (below 10 000 m/s) and deep UV lithography has reached its resolution limit ($p_{min} = 400\ nm$). Luckily there is a third possibility using the piezoelectric layer on the substrate. This configuration allows an increase in the phase velocity above 10 000 m/s by the creation of guided AW on the surface of the structure. In this case the wave is dispersive which means that the thickness of the acoustic layer has to be precisely adapted to the frequency of SAW to limit the losses.

BAW resonators are based on simple metal/piezoelectric/metal hetero-structures, in which the thickness of the piezoelectric layer and wave propagation velocity define the operation frequency, *f*, of device: $f = v/2t$, where v is the acoustic velocity in the material and t is the thickness of the film. The application of thin films in SAW and BAW structures allows the shift of operational limits towards higher frequencies of modern RF systems. AlN thin films with excellent (111) texture, a high degree of uniform polarity, and the best possible piezoelectric coupling of nonferroelectric material are currently applied in many RF BAW filters for mobile communication. Typically these films are embedded in thickness mode resonators connected together to achieve ladder-type RF filters at the carrier frequencies in the range of 1.8 to 2.2 GHz.[66,70] Their large rejection at the border of the pass band makes them ideal for duplex filters.[71] Such ladder filters also work at much higher frequencies.[72] Recently, it was discovered that partial substitution of Al by Sc – yielding the mixed solution $Al_{1-x}Sc_xN$ (AlScN) - leads to a substantial increase of piezoelectric coefficients, and piezoelectric coupling constants.[73,74] At present, AlN doping by Sc is widely studied around the world for applications in vibrational energy harvesting, high-temperature wireless SAW sensors and BAW filter applications due to the possibility for increasing by at least a factor of two the elecromechanical coupling.[75-77] The implementation of AlScN in BAW filters might be one of the possible solutions to increase the bandwidth of the filters, however the quality factor tends to decrease with Sc doping. So far the K^2 of AlScN films based BAW resonators is not high enough for ultra-wide band or high frequency filters applications.

One of the known piezoelectric materials with high electromechanical coupling is LN. Thus, it is widely used in the form of single-crystal wafers in the SAW industry. The K^2 might be as high as 53% for BAW devices based on X-cut LN.[68] Translated in terms of filters, this means that a BAW RF filter based on LN could present pass-band several times broader than that based on AlN films (**Figure 5**).[78] Alternatively, tuneable BAW filters, either based on composite structures or on the addition of tuneable capacitors inside filter circuits, need to trade K^2 for frequency tuning.[68] Starting with the large K^2 of LN-based BAW resonators, one could implement filters with conventional fractional bandwidths in the 2-5% range, while offering a tuning range in the 10-20% range of the centre frequency.[68]

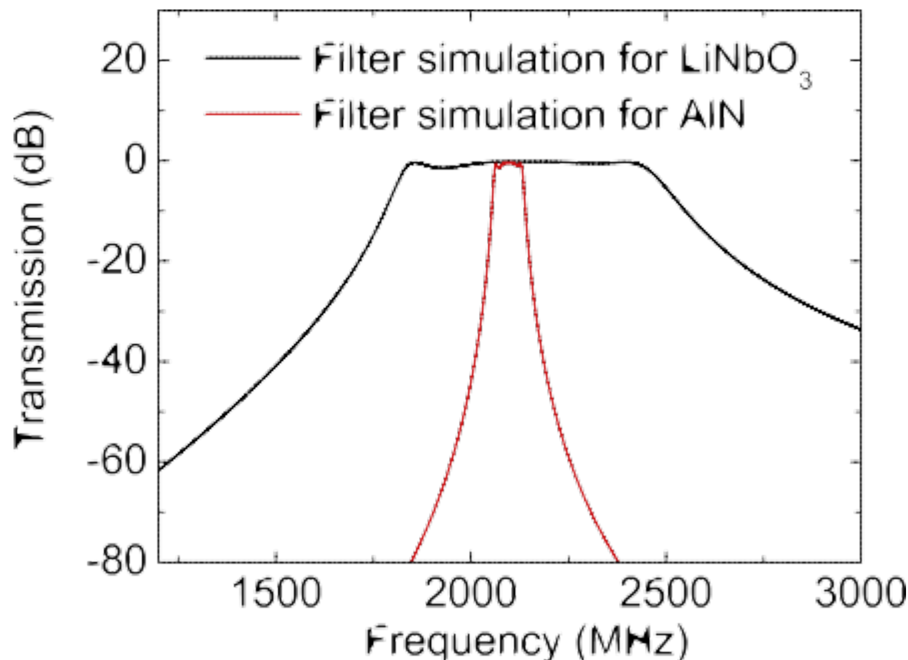

Figure 5. Comparison of the simulated bandwidth of pass band BAW filters with operational frequency around 2 GHz based on X-cut $LiNbO_3$ layer and standard sputtered AlN layer.
Reproduced with permission. [78] Copyright 2009, AIP.

1.4. Fabrication techniques of $LiNbO_3$ and $LiTaO_3$ films

LN is required in the form of thin films, due to its high K^2 (which allows for increased width of the band pass) and possible high phase velocities for guided waves (increase of the frequency). Despite the high industrial interest in LN films, the synthesis of these films is still far from routine. Although LN and LT films have been fabricated by different techniques,[79-82] many electrical and electro-optical properties reported are not comparable to those of $LiNbO_3$ and $LiTaO_3$ single-crystals. BAW devices derived from deposited c-axis oriented LN films showed a worse performance than those based on AlN.[83] The grown films presented high acoustic and optical losses (discussed in detail in part 3). So far LN is not available in the form of high quality deposited films with the required crystallographic orientation (oblique or in-plane orientation of Z-axis) on Si. At present, the techniques enabling the fabrication at the lab-scale of optical and acoustic devices are based on single-crystal LN thin films with the required orientation, are polishing or crystal ion slicing and wafer bonding techniques.[78,84] The major advantage of these techniques, based on wafer bonding and using LN single crystals as a starting material, is the free-choice of substrate material and its orientation. Both techniques help to preserve the single crystal quality of the transferred layer as confirmed by measurements of the electromechanical coupling factors with values close to those theoretically expected. The polishing and bonding fabrication method can be used to obtain LN layers with any crystallographic orientation. FBAR and HBAR with K^2 of 43% fabricated on 6.6 μm X-LN polished layer bonded on electrode/SiO_2/Si were demonstrated (**Figure 6**). The technology used to fabricate layers on the substrate so far is not sufficient to produce thin films with thicknesses less than 1 μm, has low precision in film thickness and introduces huge variations in thickness across a thin wafer. Despite very promising modelling results, the experimentally obtained transfer functions of filters based on $LiNbO_3$/Si layers, fabricated by a wafer bonding and polishing technique, still need to be improved. Experimental responses deteriorate mainly due to the inhomogeneity of the film thickness. Polishing techniques induce a large loss of material since a LN wafer needs to be ground down to leave only a thin film and this technique does not offer sufficient thickness control for commercial BAW applications. Smart-cut™, or more generally ion-slicing, is another technique, which is used for the fabrication of high quality single crystal thin films of $LiNbO_3$ on

various substrates. High quality films with thicknesses lower than 1 µm can be obtained by this technique. Ion slicing is difficult to implement on silicon due to the large thermal expansion mismatch of LN with respect to Si. So far Smart-Cut™ processing has been optimized for Z- and X-cuts of LN. A K^2 of 12.5% for SAW on transferred Y-LN films on Si was achieved.[84] Very simple BAW resonators exhibiting an electromechanical coupling factor of 53%[68] were fabricated from the Smart Cut films. These techniques, based on fabrication of LN/LT layers from the single crystal wafers, demonstrated the large electromechanical properties of lithium niobate (X- and Y-cuts). However, in the Smart-Cut BAW structures the electrode was not patterned and this limited the quality factor of the structure to 300. However, a large $Q * f$ product was obtained for the HBAR.[85] The performance of SAW and BAW devices based on LN films was reviewed by Reinhardt et al.[68] In order to obtain RF SAW devices with a reasonable price and high performance, including reproducibility, controlled thickness, high quality factor and high electromechanical coupling, the deposition of $LiNbO_3$ thin films and the fabrication of structures with a patterned bottom electrode have to be considered.

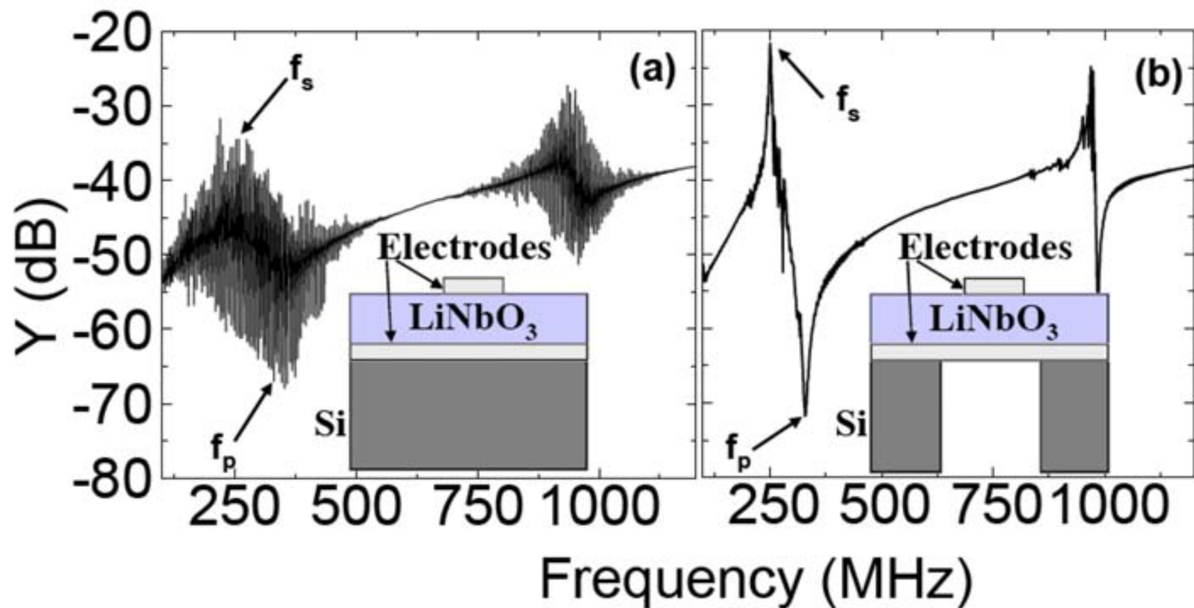

Figure 6. Frequency response of HBAR (a) and FBAR (b) based on thinned X-cut $LiNbO_3$ layer on Si. Schematic representation of HBAR (a) and FBAR (b) structures are given in the insets.
Reproduced with permission. [78] Copyright 2009, AIP.

1.5. Requirements for films applied in optics and acoustics

A special effort has to be made to obtain high quality grown LN and LT thin films with physical properties suitable for BAW & SAW RF filter and guided nanophotonic applications. To be used for these applications there are several basic requirements for the thin piezoelectric films which need to be fulfilled: a smooth surface (< 1 nm), not to be leaky or conductive, precisely controlled and homogenous thickness, homogenous and reproducible physical properties, single-domain state, crack- and twin-free, single texture or orientation, low mosaicity, reduced number of grain boundaries and defects in order to reduce propagation losses and to obtain spectral purity. There is no universal technique for the processing of advanced materials or their coatings. Usually, for each application and material more than one technique is being considered at academic and industrial levels and the final choice by industry depends on the specifications and on the maturity and readiness of the techniques. However physical vapour deposition (PVD) methods do not offer the possibility of easy control of the composition and doping, the fine adjustment of the non-stoichiometry, and the control the composition of volatile elements (such as Li_2O) in the thin films, which are the key parameters for LN and LT based technologies.

2. Growth of $LiNbO_3$ and $LiTaO_3$ films by chemical and physical methods

The first reports on the growth of c-axis oriented LN films by liquid phase epitaxy on an LT substrate and by rf sputtering on c-sapphire substrates appeared in early seventies.[31,86] Since then these substrates were widely studied for the growth of the Z-LN and Z-LT films by different methods: liquid phase epitaxy (LPE),[87] epitaxial growth by melting,[31] rf sputtering[86,88-91] pulsed laser deposition (PLD),[92-101] molecular beam epitaxy (MBE),[102] metal organic[103,104] and aqueous precursor[105-107] solutions, sol-gel,[91,108-112] spin coating,[113] microwave oven method[114] chemical vapour deposition (CVD)[115-122] and its derivatives such as thermal plasma CVD[123-126] pulsed metal organic (PMOCVD),[82] pulsed injection MOCVD,[127] spray MOCVD,[128] atmospheric pressure aerosol MOCVD,[129] solid source flash evaporation,[116] combinatorial high-vacuum CVD,[130] atomic layer deposition,[131] etc. In the following sections, we summarize the problems and the applied strategies for the optimization of growth of high quality LN-LT layers.

2.1. Crystallinity

To be applied in electrically active acoustic and optical devices and to assure high performance, LN and LT films need to be well crystallized, contain a pure $LiNbO_3$ phase and smooth surface, be twin- and domain-free, and have a high texture quality. The first task in the optimization of growth conditions is the crystallization of the layers. The main factor defining the crystallinity of grown films is the temperature. The temperature and quality of thin film crystallization depend on several factors: growth method, geometry of the growth chamber (thermal gradients, placement of thermocouples, etc.), energy of adatoms and the crystallinity, quality and energy of the substrate surface. It was observed that amorphous films on an amorphous bottom layer crystallized at higher temperatures than amorphous films grown on a crystalline base.[60,132] The crystallization of amorphous films (grown by the organometallic route) to polycrystalline LN/LT films at temperatures as low as 250°C and the films with preferred orientation on sapphire substrates at 400-500°C was reported.[132,133] Slow crystallization of the polycrystalline state of sputtered films was observed during post-growth annealing at 460°C, while this process was quite fast at 600°C.[134] The high surface mobility of adatoms is required for the epitaxial growth. Temperatures used for epitaxial growth were much higher than those applied to crystallize the amorphous layers or the growth of polycrystalline films. In the case of CVD techniques, the deposition temperatures around 400-450°C resulted in incomplete oxidation and carbon residues in the films.[115] The epitaxial quality is improved by the increase of the growth temperature.[116] However, at high temperatures (> 750°C) volume reactions take place in CVD processes which reduce the texture quality.[116,135] Epitaxial films were obtained by annealing at 650°C for 15 min the amorphous LN layers grown by ALD at 235°C.[131] Deposition temperatures of 500 - 800°C were used for the growth of epitaxial LN layers by physical deposition methods (PLD, rf sputtering, etc.).[136,137] To grow high quality LT films, higher deposition temperatures have to be used than those used for LN films due to the very high melting temperature of LT (LT ~ 1650°C and LN ~ 1250°C).[138] High quality epitaxial LT films have been obtained at temperatures higher than 780°C by PLD.[138]

2.2. Compositional analysis

The difficulty of control of the alkaline element composition in alkaline niobate thin films is one of the major limitations to their applications.[139] As mentioned above, lithium is a light element and its oxide is volatile at high temperatures and in vacuum conditions. Numerous publications were dedicated to the elimination of the formation of the Li-poor or Li-rich secondary phases (($LiNb(Ta)_3O_8$ or $Li_3Nb(Ta)O_4$) and to optimize the growth of single-phase LN/LT films. The standard technique used for phase compositional analysis of LN/LT films is X-

ray diffraction (XRD).[118,140-142] In the case of a system containing two phases, the orientation of the inclusions of the secondary phase in the film matrix is defined by the minimum of the interface energy.[143] The $LiNb_3O_8$ phase grows epitaxially in three dimensions in the LN matrix, regardless of the LN orientation. The epitaxial relationships between $LiNb_3O_8$ and LN lattices are $(010)_{LiNb3O8}||(2\bar{1}\bar{1}0)_{LN}$ and $(\bar{1}01)LiNb_3O_8||(0001)LN$.[143] The single symmetry plane of $LiNb_3O_8$ coincides with the three mirror planes of LN. In the case of c-axis LN films, precipitations of monoclinic $LiNb_3O_8$ with $(\bar{6}02)$ planes parallel to the surface and (111) textured Li_3NbO_4 phase were identified.[89,144] Moreover, $(\bar{6}02)$ $LiNb_3O_8$[89] and (111) Li_3NbO_4 have good lattice matching with c-sapphire. When the volume fraction of this secondary phase in C-LN films was small, asymmetric profiles of XRD reflections have often been observed.[127,141] In the case of thin films, asymmetric profiles of XRD reflections are very common and may originate from gradients in composition or residual stresses as well as the presence of the secondary phases. Consequently, this may lead to misleading conclusions about the phase composition of textured LN/LT films. Therefore, other XRD techniques such as reciprocal space,[95] 2Θ-ω mapping,[145] and tilt-angle[80] XRD have been used for the identification of parasitic phases in thin films. However, these methods are time consuming and the volume fractions of less than 3 mol% cannot easily be identified in thin films. Thus, it is essential to use methods complementary to XRD, such as Raman spectroscopy, which is a very sensitive and fast technique for the detection of the parasitic phases with different symmetries.[127] In the case of LN and LT films and crystals, Raman scattering is used as a non-destructive, local and fast probe for strain, Li non-stoichiometry and $LiNbO_3$ phase purity.[127,129,146,147] Additional Raman modes to the LN Raman signature have been observed in thin film spectra and they were interpreted as defect modes, mainly related to the Li deficiency.[148,149] Later, the frequencies of Raman modes of $LiNb_3O_8$ and Li_3NbO_4 were identified and these modes were attributed to the $LiNb_3O_8$ phase.[127] In the case of $(01\bar{1}2)$ oriented films, the reflections of parasitic phases with a low volume fraction were not observed in standard Θ/2Θ patterns although the presence of the secondary phases was confirmed by 2Θ-ω maps[145] or Raman spectroscopy.[127] It is worth noting that Raman spectroscopy is a local method, thus Raman mapping is highly recommended in phase compositional analysis as secondary phases tend to segregate.[127]

To obtain high-performance LN-LT films, deposition of a single-phase film is a necessary but not sufficient condition. Frequently, single-phase LN-LT films were labelled incorrectly as stoichiometric films in literature. It is important to note that the LN and LT phase exists over a wide compositional range (as described above). Thus, the films with Li_2O concentration lower than 50 mol% are nonstoichiometric although they consist of a single phase. Different direct methods such as the secondary ion mass spectroscopy (SIMS),[93,117] X-ray photoelectron spectroscopy (XPS),[150,151] ICP-AES,[118,136] and Rutherford backscattering spectrometry (RBS)[152,153] were used to estimate Li concentration within the grown films. The Li concentration cannot be estimated directly from RBS data, thus the Nb/O ratio was studied, which makes analysis highly inaccurate.[153] The combination of RBS with nuclear microanalysis of Li and O content made it possible to determine the absolute film composition with an accuracy of 3% for Nb and O and of 10% for Li, and the relative element ratios with a precision of 1%.[154] The accuracy of XPS in Li concentration is within 20%.[151] A 1-2% error in absolute Li concentration can be attained by ICP-AES.[118] However, the control of LN/LT film composition with precision of 1-2% is not sufficient for industrial applications due to a strong variation of their physical properties as a function of Li non-stoichiometry. Many reports make claims of high quality LN or LT films obtained by PLD,[101,155] MOCVD,[116,121,156,157] and sputtering,[137,158] but very few reports were found giving a precise estimate of Li concentration and dealing with stoichiometry in LN-LT thin films in detail. The application of indirect methods, used for compositional analysis of LN/LT single crystals (discussed above), to thin films is complicated by the fact that the physical properties of the thin films are highly dependent not only on the non-stoichiometry but also on the residual stresses and the defects present (grain boundaries, dislocations, structural defects, etc.). The refractive indices seem to be more affected by the film structure and texture quality than by the Li non-stoichiometry.[159] Several papers report on Li content within the film estimated from lattice parameters,[95,120] Curie temperature,[146,151] or Raman mode damping,[160]

but they do not take into account the strain which may affect these properties as well. The effect of the Li deficiency on the lattice parameters is negligible with respect to that of residual stresses in epitaxial LN/LT films.[129] Thus, XRD data can be used for the estimation of the residual stresses with reasonable accuracy without taking into account the effect of Li composition in the films but is not recommended for compositional analysis of films. The effects of residual stress and Li deficiency were decoupled in the analysis of the non-stoichiometric LN/LT films by combining Raman spectroscopy and XRD analysis and by doing calibrations of uniaxial stress and non-stoichiometry effects on the Raman mode damping and wavenumbers.[146] An accuracy in Li_2O concentration of 0.1 - 0.2 mol% can be achieved by this method if the local standard of congruent LN/LT crystal is used to calibrate the Raman measurements and if the crystalline quality of the films is very good.[129,146]

2.3. Control of Li non-stoichiometry and composition in thin films

As discussed above, the deficiency in Li tends to decrease the electromechanical coupling slightly (0.4% per mol% of Li_2O).[18] The acoustic velocity and optical properties are also highly dependent on the Li non-stoichiometry. Therefore, the control and optimisation of the Li_2O non-stoichiometry in films will be a key factor in obtaining high performance and reproducible acoustic and optical signals in devices based on LN/LT films.

Physical methods, such as PLD and rf sputtering, may provide high quality epitaxial films, but Li loss is considerable in these techniques due to scattering processes during the expansion regime which is dependent on the mass of gas[160] and high Li_2O volatility at high temperatures in vacuum.[136,161] Son et al.[141] and Gonzalo et al.[160] have carried out parametric studies, which have indicated that the light Li species were scattered by buffer gas. Thus, the films grown at high target-substrate distances or off-axis were rich in Li while the small distance and in-axis growth resulted in Li-poor compositions. These observations were described by an analytic kinetic model predicting the spatial and temporal evolution of the population densities of Li species in laser generated plasmas.[162] To compensate these Li_2O losses, several approaches have been adopted in the literature: use of Li-rich targets, deposition at low temperatures and/or at high pressure.[136,137,161,163] In the case of PLD and rf sputtering, the growth of single-phase films has been achieved by optimising the deposition temperature, rf power or laser fluence, target composition, total gas pressure, oxygen partial pressure, target-substrate distance and orientation.[98,137,138,141,154,160] The Li content in the films, grown by PLD and rf sputtering, increased with the increase of partial oxygen pressure, total pressure, rf power or laser fluence.[137,141,145,159,160,164] The high pressure, of a reactive or inert nature, results in the same effect –focusing the expanding Li species and the increase of Li content in the films.[160] Contrary results have been reported by Shibata et al.[98,138] They have observed the highly inhomogeneous angular distribution of ablated Li and Nb species but with the homogeneous central zone containing the Li/Nb ~ 1 which had a diameter of less than 10 mm and the external zones were low in Li (Li/Nb ~ 0.5). Moreover, the Li concentration in their films decreased with the increase of the deposition pressure and partial oxygen pressure. The composition of films deposited by PLD and sputtering was highly dependent also on the target quality (single crystal, sintered ceramics or pressed powder).[165,166] Furthermore, the phase composition was dependent on the substrate and its orientation.[145] To summarize, the deposition of compositionally homogenous LN and LT films by means of physical methods is very challenging due to the inhomogeneous distribution of Li species in the created plasma and high Li_2O losses at high temperatures. Although the high quality single-phase LN/LT films on small substrates for scientific purposes have been obtained, the huge spatial inhomogeneity of composition is not suitable for the industrial processing requiring films with homogeneous properties on the wafers with diameters of 100 - 150 mm.

Better control of volatility and composition of alkaline elements can more easily be achieved by chemical deposition methods, such as spray pyrolysis, MOCVD, sol-gel and ALD, in which the film composition can be easily modified by the modification of ratios of element

precursors. Amorphous films of LN, LT and LN-LT solid solutions or organic films containing Li-Nb(Ta) were deposited on sapphire, LN/LT and MgO/Si substrates by means of sol-gel,[111,167] MO decomposition (MOD),[103,133,168-170] polymeric precursor,[171] aqueous solution,[106] microwave oven,[114] or ALD[131] methods at low temperatures. Then epitaxial or highly textured LN/LT films were obtained by annealing these layers at 500-900°C. Although these low cost methods can be scaled up, simplify the control of Li composition in the layers and are cost-effective, the epitaxial quality of the films needs further optimisation. The crystallization of the amorphous layers involves two competing processes: epitaxial crystallization on the substrate surface and random nucleation in the film volume and the surface.[128] Thus the epitaxial and texture quality is usually lower for films prepared by solid-phase epitaxy than for films grown epitaxially from the vapour phase directly. For example, the full widths at half maximum (FWHM) of the rocking curves of (0006) reflections of c-axis oriented LN films on sapphire grown by the MOD and polymer precursor method were 0.8° and 1.2° respectively.[169,171] Epitaxial LT films deposited on sapphire by MOCVD at 750°C had a FWHM of 0.2°.[172]

The industrial requirements (cost, quality and reproducibility) for high quality epitaxial films, demanded for acoustic and optical applications, can be satisfied by chemical deposition methods, such as versatile MOCVD, which is already commercialized and is suitable for large area depositions with homogeneous thicknesses (± 1%) and composition. In thermally activated CVD, the epitaxial growth takes place at higher deposition temperatures (> 650°C) than in the physical methods). The window of vapour compositions which permits the growth of single-phase epitaxial LN/LT films becomes larger at higher temperatures as well.[118,142] However at high temperatures (> 750°C) volume reactions occur in CVD which impair the quality of the growing film. The main disadvantage of conventional MOCVD systems is that the vapours are generated by heating powder or liquid to a high temperature. It is difficult to control and adjust the evaporation of precursors with different thermal properties and volatilities, such as precursors of alkaline elements (Li) and those of Nb/Ta, and to keep the flow of each element vapour to the reaction chamber constant. Organometallic precursors of Li have a low vapour pressure.[119] Several different modifications of conventional MOCVD have been used to grow LN and LT films: solid source flash evaporation,[116] pulsed-injection MOCVD,[82,146] spray-MOCVD,[128] combinatorial high-vacuum CVD,[130] pyrosol-atmospheric pressure MOCVD,[129,173] and thermal plasma spray CVD.[124] For pulsed – injection (PI), liquid injection or spray MOCVD, the vapour phase is generated by the flash evaporation of a solution containing a mixture of metalorganic precursors. The solution is kept at ambient conditions during the process and small amounts of solution are fed into the hot evaporator. In this way the volatility of Li precursors is improved and the composition of alkaline elements can more easily be controlled by these techniques than by conventional MOCVD methods. Nearly stoichiometric composition of LN and LT films has been achieved by these methods (**Figure 7**).[146,174]

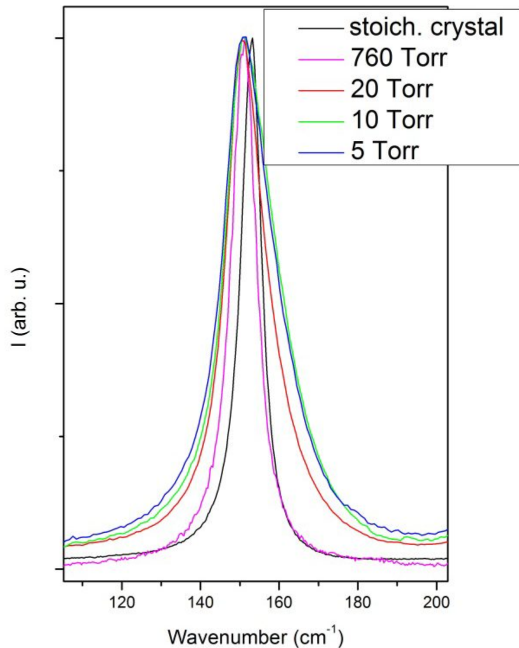

Figure 7. Comparison of E(1TO) Raman mode profile of $LiNbO_3$ films on C-sapphire grown at different pressures (ranging from 5 to 760 Torr) by MOCVD with the E(1TO) mode profile of stoichiometric Z-cut $LiNbO_3$ crystal. It indicates that nearly stoichiometric films can be grown by CVD techniques.
Reproduced with permission. [174] Copyright 2013, SPIE.

The quality, compatibility and efficiency of the precursor materials are the key factors determining the quality of grown films and the reproducibility of chemical methods. Diketonate and alkoxide precursors of Li, Nb and Ta have been used for the growth of LN-LT films. Deposition conditions used with these precursors in CVD of LN and LT are summarized in **Table 2**. Saulys et al. have studied the decomposition chemistry of Li and Nb diketonates and alkoxides.[175] It was found that the metal alkoxides had better thermodynamic stability than diketonates, which started to decompose at room temperature in vacuum.[175] Therefore diketonates are not suitable for conventional MOCVD using solid sources. However $[Li(OBu^t)]_6$ is highly susceptible to hydrolysis and generates LiOH, which contributes to highly reduced growth rates above 500 °C.[175] Feigelson has claimed that the process using niobum ethoxide had very poor reproducibility for solid-source flash evaporation MOCVD and it was preferable to use the diketonate precursors with the same ligand (Li(thd) and $Nb(thd)_4$, where thd stands for 2,2,6,6-tetramethyl-3,5-heptandione).[116]

The composition of layers deposited by CVD depends on the partial pressures of the Li and Nb (Ta) source precursors, their decomposition chemistry and the volatility/desorption of Li_2O from the growing layer. The Li_2O evaporates during the post-growth annealing, as well.[129] The Li_2O loss depends on the temperature, annealing duration, layer thickness and its stoichiometry.[129] The stoichiometry of the growing layer also depends on other deposition conditions, such as total pressure and temperature.[174] In the case of CVD, the Li content in the films is adjusted roughly by adjusting the Li/Nb ratio in the precursors and then the stoichiometry can be finely tuned by varying other deposition conditions. To ensure the stoichiometric composition of the LN/LT layers grown it was suggested using double-alkoxide precursors, containing Li-Nb or Li-Ta elements in the same molecule.[82,120,176] LN films grown using single source precursor at 600°C contained a secondary phase, which might be related to the dissociation of the precursor.[119] Thus, to avoid Li_2O loss during film growth, amorphous LN-LT films were grown at low temperatures (450°C) from single-source precursors, synthesized by reacting Li(thd) and $Nb(OC_2H_5)_5$ (or $Ta(OC_2H_5)_5$) and then the films were annealed at 700 °C.[128] To improve the epitaxial quality of these films a two-step process was optimized.[177] Xie et al. have reported the growth of single-phase films from the lithium tantalum hexa-t-butoxide

directly at 700°C by means of liquid injection MOCVD.[82] Double alkoxide precursors have been used also for the growth of LN-LT solutions with controlled Ta/Nb ratio.[124,126] Unfortunately, the Li non-stoichiometry was not studied in these films by means of indirect methods and it remains unknown if the films were stoichiometric when single-source precursors were used.

2.4. Control of texture and in-plane orientation

To be useful in targeted acoustic and optical applications, LN and LT thin films have to present a specific orientation, adapted to the requirements of the targeted application. To ensure single mode behaviour and low propagation losses, devices based on SAW, Lamb or optical waves require a proper propagation direction in the substrate plane. Thus the films used in these devices should present single out-of- and in-plane orientations. Textured films without preferential in-plane orientations can be used for the BAW devices, in which the waves are excited across the film thickness, pyroelectric sensors and energy harvesters. Polycrystalline LN and LT films do not present real potential in acoustic, optical, pyroelectric and energy scavenging applications.

Single crystalline substrates and the buffer layers were identified for the epitaxial/textured growth of X-, Y-, Z- and (012) orientations of LN and LT films. Very little is known about the possibility of epitaxially growing other orientations of LN/LT. The $(10\bar{1}1)$ texture of LN films was revealed on (200) MgO substrates as indicated by theta/2theta XRD pattern.[178] However in this paper the authors claimed that films had a polycrystalline nature. It is important to note that 100 mm and 150 mm diameters are standard sizes for wafers used in the SAW/BAW industry, which allows the fabrication of many filters on the same substrate and reduces their price. In the case of waveguide applications, the substrate must have a lower refractive index than LN/LT. Thus the bulk of work has been done on the optimization of the LN/LT growth on sapphire, silicon and LN/LT substrates. At present the silicon based technology is widely used for 300 mm diameter wafers, and the introduction of 450 mm diameter wafers for mass production is under discussion.[179] Sapphire and LN/LT substrates are relatively cheap and available with diameters up to 200 mm and 150 mm, respectively. Other substrates such as quartz, glass, and single crystal oxides (MgO, $SrTiO_3$, and $LaAlO_3$) have been considered as well. However, it would be difficult to implement the epitaxial LN films on single crystalline substrates (such as sapphire, $LaAlO_3$ or $SrTiO_3$) for industrial processing of RF filters. $LaAlO_3$ and $SrTiO_3$ crystals are very expensive and the size of wafers available is too small (2-3 inch diameter).

2.4.1. (0001) orientation

LN and LT films oriented with the polarization axis perpendicular to the substrate plane have been extensively studied in the literature for their potential applications in electro-optics. LN and LT are isotructural materials and the mismatches between their a- and c-axis are 0.3% and 0.6% (**Table 3**). Sapphire crystals ($R\bar{3}c$ space group) have a very similar structure to that of LN and LT crystals (space group R3c). The lattice mismatch between LN (LT) and sapphire is significant (-8.2% (-8.2%) along the a-axis and -6.6% (-5.9%) along the c-axis) (Table 3). Therefore, the films relax the high misfit strain by formation of misfit dislocations at the film/substrate interface. The high mismatch between the substrate and the film introduces mosaicity and complicates the growth of films (especially thick films) with very high crystalline quality. Nevertheless, C-sapphire substrates are one of the most studied substrates for the epitaxial growth of the LN and LT films. Epitaxial LN layers on C-sapphire were grown in the temperature range from 550°C to 800°C by chemical and physical deposition methods.[90,92,95,116] In the case of MOCVD, the range of vapour compositions allowing epitaxial growth of the pure LN phase is broader at higher temperatures.[118] The texture quality of the films was highly dependent on the deposition temperature and other deposition conditions. The lowest mosaicity of C-LN films on C-sapphire was obtained at deposition temperatures around 700°C.[116,180] At low deposition temperatures, the atom mobility is too low on the surface to form a highly ordered crystalline lattice. Increasing the CVD temperature above 700°C resulted in the

degradation of mosaicity due to pre-reaction of the precursors in the reactor volume and the increased number of particulates that attached to the surface.[116] The epitaxial relationship of LN with C-sapphire is ($(0001)_{film}||(0001)_{Al2O3}$ and $[11\bar{2}0]_{film}||[11\bar{2}0]_{Al2O3}$. Frequently C-LN films, especially when grown at low temperatures, contained 180° rotated growth domains ($[11\bar{2}0]_{film}||[\bar{1}\bar{1}20]_{Al2O3}$), which can be obtained by rotating the hexagonal cell by 180° or 60 °around the c-axis (**Figure 8**). It is important to note that both angles are used to define these domains and sometimes growth domains are called twins in the literature. In this paper we distinguish between the terms of growth domain, twin and ferroelectric domain, as they have different origins. Growth domains result from the several ways the layer lattice can attach to the substrate surface. Usually the boundaries between the growth domains are defective (**Figure 9**).[122,135] Twins may exist in films and single crystals. They form to relax the stresses related to thermal or compositional gradients in single crystals or to the mismatch between the lattices or thermal expansions of the films and the substrate. The twins are shearing one lattice plane with the remaining matrix, thus the twin boundaries with the matrix are defect-free (Figure 9).[121] Ferroelectric domains in LN and LT are related to the ferroelectric polarization axis direction and they can be represented by (0001) and $(000\bar{1})$. The defects on the ferroelectric domain walls are related to the movement of ions due to the internal electric fields present or due to the pinning of the walls on the defects in the lattice. The growth of 180° domains in C-LN/LT films are slightly less energetically favourable than the domains with $[11\bar{2}0]_{film}||[11\bar{2}0]_{Al2O3}$ due to the reduced distance between the Al, Li and Nb on the oxygen terminated sapphire surface at the film/substrate interface, as explained by Lee et al. (**Figure 10**).[135] The volume fraction of these domains was reduced at higher deposition temperatures, a lower growth rate and smaller lattice mismatch between the substrate and the film.[116,135] At low temperatures or high deposition rates, the surface mobility is low and the growing lattice is not able to adopt the orientation with the lowest energy. For CVD processes the growth domains may reappear at deposition temperatures higher than 750°C due to a volume reaction and the related formation of defects.[116] The formation of 180° rotated growth domains has never been observed in LN/LT films on LN or LT substrates. The volume fraction of this secondary orientation can be eliminated by post-annealing at temperatures ≥ 750°C.[181]

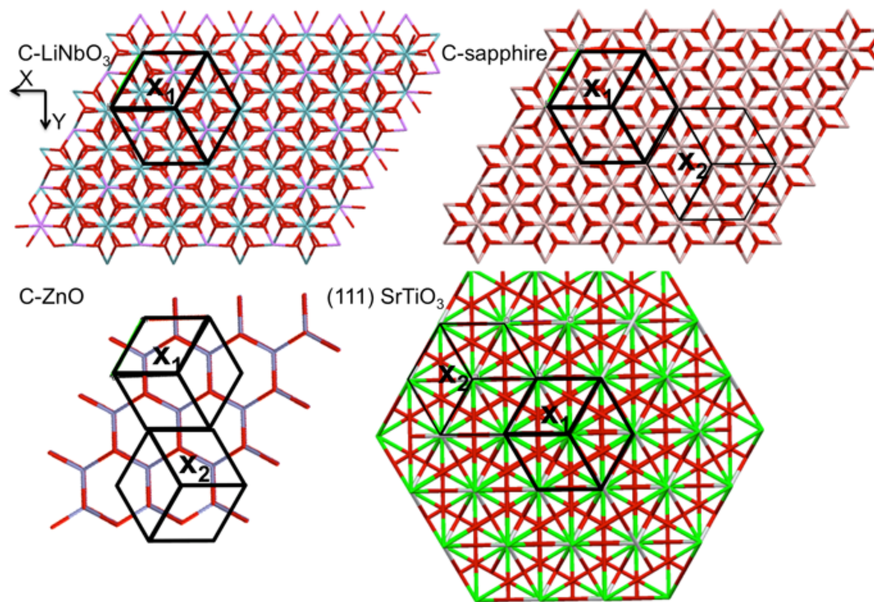

Figure 8. Schematic representations of the surface structures and the orientation(s) of the unit cell of C-$LiNbO_3$ or C-$LiTaO_3$ grown epitaxially on the surface of the C-$LiNbO_3$ (or C-$LiTaO_3$), C-sapphire, C-ZnO and (111) $SrTiO_3$. The main orientation (X_1) of the growth domains with better lattice matching is shown in bold.

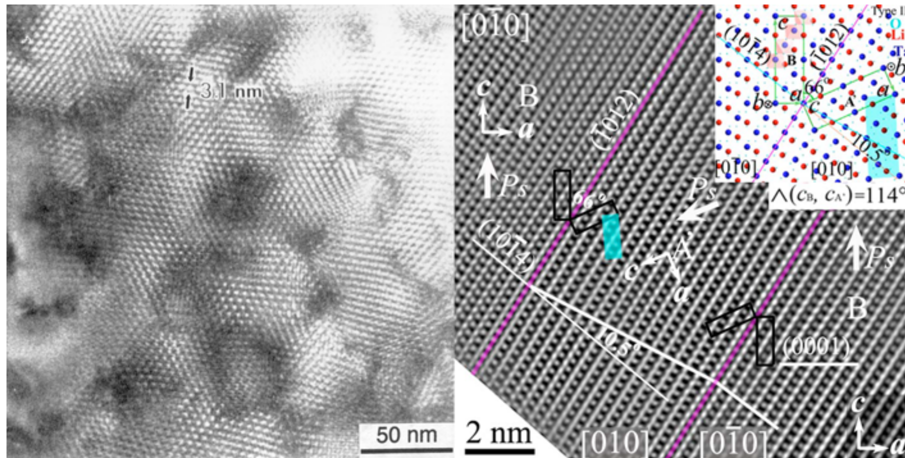

Figure 9. A high resolution plane view TEM image of C-LiNbO$_3$ film on a C-sapphire substrate, showing defective grain boundaries between the 180° growth domains (left hand image). Reproduced with permission. [135] Copyright 1998, Elsevier. Fourrier –filtered high resolution TEM image of a C-LiTaO$_3$ film on C-sapphire, corresponding to a defect-free twin boundary (right image). Reproduced with permission. [121] Copyright 2009, AIP.

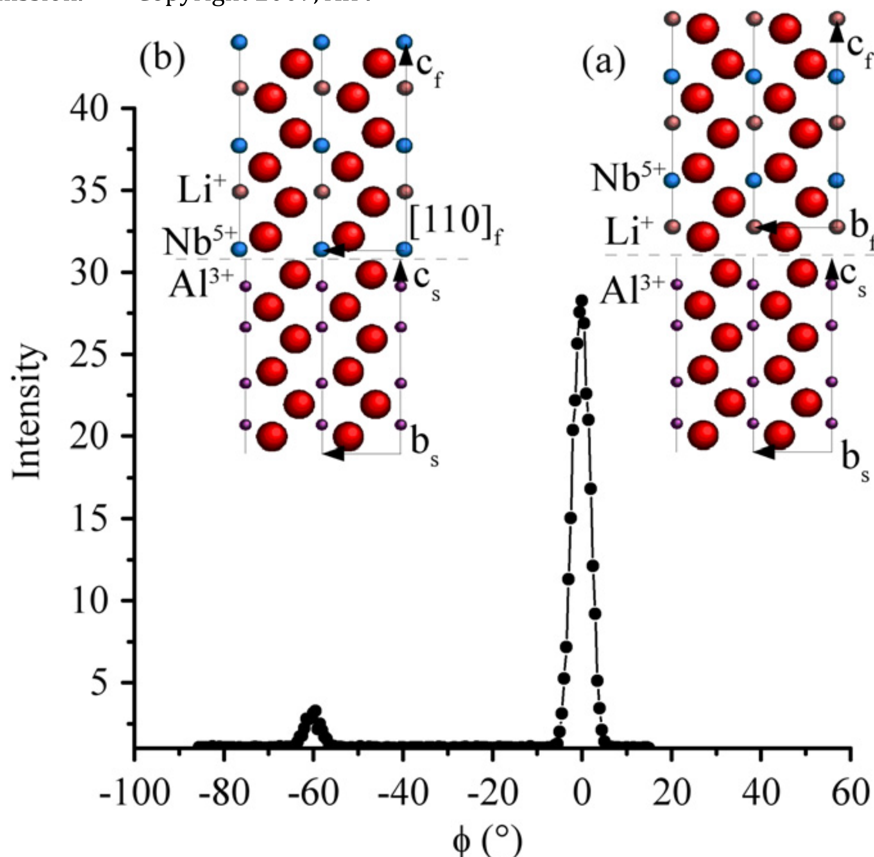

Figure 10. φ-scan of the (0 1 8) reflection of LiNbO$_3$. The reflection at φ = 0° corresponds to the epitaxial relationship [11-20]$_{film}$||[11-20]$_{Al2O3}$. Schematic representation of the interface matching (indicated by dashed line) between the sapphire and the main orientation of LiNbO$_3$ film (a) and the growth domain rotated by 180° in the substrate plane (b).
Reproduced with permission. [95] Copyright 2009, IoP Science.

LaAlO$_3$ (LAO) is isostructural with sapphire (R$\bar{3}$c space group) and has similar lattice parameters (Table 3). This substrate is very popular for the growth of layers with the perovskite structure. Its orientations are usually described in pseudo-cubic settings. (0001) planes in the hexagonal cell are named (111) planes in the cubic setting. The hexagonal cell will be used for LaAlO$_3$ in this paper. The in-plane lattice parameters of C-LaAlO$_3$ is larger than those of LN and LT and the lattice mismatch between C-LN(LT) and C-LaAlO$_3$ substrate is smaller (around 4%)

than that in C-LN/C-sapphire hetero-structure. The growth of c-axis oriented LN/LT films on this substrate was not reported in the literature. This substrate shows few possibilities for integration with the industrial fabrication of films and devices because it is quite expensive, available only in wafers with small diameters and presents elastic twins.

Hexagonal c-axis oriented ZnO layers have been used for the growth of epitaxial or textured LN/LT films. ZnO layers as bottom and top layers for LN/LT films are attractive for several reasons. ZnO displays preferential growth along the c-axis, so c-axis textured ZnO films can be obtained on any substrate including amorphous layers such as SiO_2 and substrates with a large lattice mismatch.[182-184] In the XY plane, the unit cell of LN/LT (in hexagonal settings) is well matched to the hexagonal cell of ZnO rotated by 30 ° around c-axis (a misfit strain of +8.4% along X- and Y-axis, Table 3, Figure 8).[185-187] C-ZnO can be used as a template layer on any substrate to initiate LN/LT growth along the c-axis. Conductivity in ZnO can be induced by doping with Al (Al:ZnO). Al:ZnO can be used as a transparent bottom electrode for devices, measurements of electrical properties and electrical poling of layers.[97,148] ZnO can be etched very easily with any acid and this makes it attractive for the fabrication of LN/LT membranes.[188,189] ZnO has a lower refractive index than LN/LT and can be used as a buffer and/or cladding layers in the waveguides based on LN/LT films.[187] ZnO has a hexagonal structure which induces the unavoidable formation of 180° in-plane rotated growth domains in LN/LT layers with $[11\bar{2}0]_{film}||[10\bar{1}0]_{ZnO}$ and $[11\bar{2}0]_{film}||[\bar{1}010]_{ZnO}$ (Figure 8).[185] C-axis oriented LN films have been also grown on $Al_{1-x}Ga_xN$ and GaN semiconductor buffer layers mainly on sapphire substrates[190-193] AlN, GaN and their solid solutions have the same structure as ZnO and even better lattice matching with LN (AlN - 4.4%, GaN – 6.7%, Table 3) than ZnO (8.4%). The LN layers had the same 30° rotated epitaxial relationship with AlN-GaN as with ZnO.[191,192]

Epitaxial (0001) oriented LN and LT layers have also been grown on cubic substrates. (111) oriented cubic substrates have a three-fold symmetry in the plane. They offer the possibility of growing epitaxial LN and LT films with single in-plane orientation as in the case of rhombohedral substrates of sapphire and LAO (Figure 8). Epitaxial growth of LN/LT on cubic substrates has hardly been studied. MgO substrates received some attention due the low refractive index (n=1.73) and the possibility to create efficient optical waveguides.[194] However, MgO reacts with humidity and carbon dioxide at ambient conditions and hermetic packaging or protective layers are required for devices based on MgO. The distances between the $(30\bar{3}0)$ and $(11\bar{2}0)$ planes of LN are well matched to the single distance between $(2\bar{2}0)$ planes and the triple distance between $(22\bar{4})$ planes of MgO, respectively (mismatch of 0.2%).[194,195] Epitaxial (111) MgO buffer layers were applied to grow highly oriented LN and LT films on (111)GaAs substrates [196,197] LN and LT films grew epitaxially with the c-axis oriented perpendicular to the MgO/GaAs substrate plane. The mosaicity of the films was around 1° and the in-plane misalignment was of several degrees.[196] The texture quality of LN/LT layers was mainly limited by the quality of MgO buffer layer. Similar to LN/LT films on sapphire, growth domains, rotated by 180° in the substrate plane, were identified in films on (111)MgO substrates[194] or buffer layers.[196,197] Although the epitaxial quality of LN/LT layers on MgO/GaAs was not very good, the films contained well defined X, Y and Z-axes, which is particularly important in the functionality of the films. The epitaxial growth of C-LN films was possible directly on (111) GaAs substrates with $[10\bar{1}0]$ and $[11\bar{2}0]$ axes of LN aligned on the [110] and [211] directions of GaAs, respectively. The insertion of a chemical buffer layer at the interface between GaAs and LN/LT is required, as GaAs chemically reacts with LT and LN at high temperature.[197] Commonly used substrates, such as $SrTiO_3$ and LSAT ($(LaAlO_3)_{0.3}(Sr_2AlTaO_6)_{0.7}$) with a (111) orientation, are potential substrates for high quality epitaxial Z-axis oriented LN and LT films as they have quite well matched in-plane lattice parameters (Table 3). Textured or epitaxial LN/LT films can be obtained on the (111) Pt layers. The distance between $(2\bar{2}0)$ is equal to twice the distance between $(11\bar{2})$ planes in the Pt structure. Growth domains rotated by 90° around the surface normal (exchange between X- and Y-axis) can be expected, in addition to 180°-domains.

Z-axis oriented LN and LT films were grown epitaxially on the (100) YSZ substrates. The $(11\bar{2}0)$ LN/LT planes match perfectly to the (020) planes of YSZ (0.2% misfit strain, Table 3)). The lattice mismatch along the Y-axis of LN/LT is 15.7%. Four orientations of growth domains,

rotated by 90° around the c-axis of LN, co-exist with similar volume fractions due to the four-fold symmetry of the (100) plane of YSZ (calcium fluorine type, cubic face centered: $(Zr,Y)O_2$ with ZrO_2:Y_2O_3 = 92:8)(**Figure 11**). The grain boundaries of 90° domains should contain many more defects than those of 180° domains as two grains with different crystallographic orientations have to be joined. For the growth of Z-LN/LT films, cubic substrates with (111) orientation are preferable.

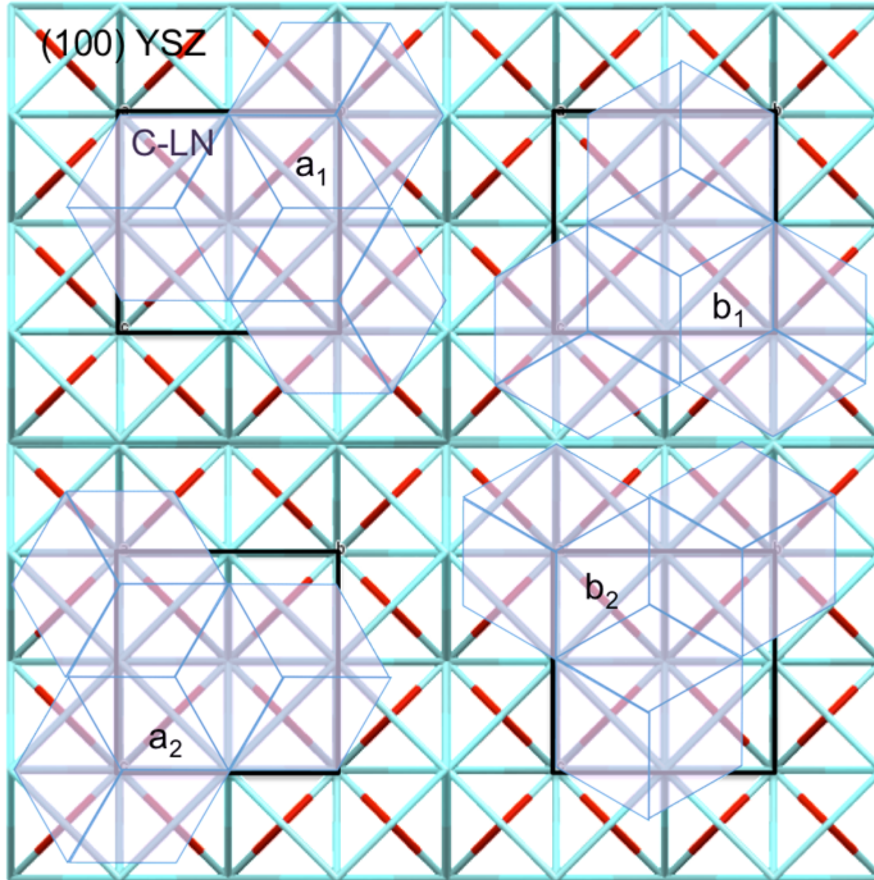

Figure 11. Schematic representation of four in-plane orientations (a_1, a_2, b_1, b_2) of the unit cell of C-$LiNbO_3$ or C-$LiTaO_3$ grown epitaxially on the (100)-YSZ substrates.

2.4.2. $(11\bar{2}0)$ ORIENTATION

The $(11\bar{2}0)$crystallographic plane is labelled the A-plane in the hexagonal cell, which is taken parallel to the mirror plane. The a-axis of the hexagonal system is called the X-axis in orthogonal settings. To grow LN and LT films with their X-axis perpendicular to the substrate plane, A-sapphire and X-LT substrates have been used. Epitaxial X-LN and LT films were grown by PLD,[136,155,161,163] rf sputtering[198] and CVD[117]. LN and LT films with preferential $11\bar{2}0$ orientation and on A-sapphire were obtained by dip coating[132] sol-gel/spin coating[199] and MOD methods.[168] As mentioned above, LN and LT lattices are isostructural and with very close interplanar distances, thus their lattices tend to align during epitaxial growth. The lattice mismatch between $(30\bar{3}0)$ and (0006) planes of X-LN and X-LT are 0.07% and 0.70%, respectively. Very small difference in lattice size of LN and LT made it possible to obtain high quality LN films on LT substrates.[117] The first growth of epitaxial X-LN films on sapphire was carried out by means of PLD.[136] It was reported that A- and C-domain growth was competing on A-sapphire and that LN films with single a-axis orientation could be obtained at low oxygen pressure during PLD deposition.[136] Later it was reported that the film orientation could be changed from c-axis to a-axis by tuning other deposition parameters, such as total pressure, laser beam energy, etc.[155] The epitaxial in-plane relationships between X- and Z-LN films and A-sapphire (out-of-plane orientations $(11\bar{2}0)_{film}||(11\bar{2}0)_{Al2O3}$ and $(0001)_{film}||(11\bar{2}0)_{Al2O3}$,

respectively) is $[0001]_{film}||[0001]_{Al2O3}$ and $[11\bar{2}0]_{film}||[0001]_{Al2O3}$ (**Figure 12**).[136,155] Sapphire substrate has a smaller unit cell, described in hexagonal settings, than LN and LT. Thus X-LN (X-LT) films growing on A-sapphire are under a compressive strain of -8.22% (-8.15%) and -6.65% (-5.91%) along the Y- and Z-axis, respectively (Table 3). The mismatch between $(10\bar{1}4)$ planes (also perpendicular to the substrate plane) of LN and sapphire is 7.4%. For C-LN films on A-sapphire, the distance between three $(30\bar{3}0)$ planes of LN matches the distance between two (0006) planes of sapphire (2.6% mismatch) and one distance between $(11\bar{2}0)$ LN planes fits the two interplanar distances between the $(30\bar{3}0)$ planes (6.3%). The $(01\bar{1}2)$ planes of C-LN are very well matched (1.9%) to the $(10\bar{1}4)$ planes of A-sapphire. Although one unit cell of C-LN is a better fit on the A-plane of sapphire than that of X-LN, A-sapphire does not show the three-fold symmetry in the substrate plane. Thus, the unit cells of C-LN, rotated by 120° and 240° around the c-axis with respect to the well-matched first LN cell, have to adapt to a large mismatch (14.5%) of the Y-axis with the $(01\bar{1}2)$ family of planes of sapphire (Figure 12). The interfacial energy of C-LN/A-sapphire is higher than that of X-LN/A-sapphire.[155] The interface energy E_i, is defined by $E_i = \sigma_s + \sigma_f - \gamma$, where γ is the cohesion energy resulting from the formation of the interface, σ_s and σ_f are free energies of the substrate and film surfaces, respectively. Higher cohesion energy of the specific plane with the substrate plane will favour its epitaxial growth. The key factors determining the preferred plane for the epitaxial growth is the adatom energy and substrate and film surface free energies during the nucleation stage. The C-plane of LN is much denser than the A-plane so it has a lower surface energy. Lower adatom energy represents a lower mobility and increased difficulty in adapting to the best matching cell in the long-range scale. This explains why c-axis oriented LN films on A-sapphire were obtained at high oxygen pressures or reduced laser fluence which resulted in low adatom energies and made the free surface energy a dominant factor.[155] The c-axis oriented LN films on A-sapphire consisted of growth domains which were rotated by 180° around the c-axis with respect to each other. The volume fraction of growth domains should be very similar as the mismatches between the interplanar distances of these domain with those of the A-plane of sapphire are equivalent (Figure 12). The epitaxial quality of c-axis oriented films on A-sapphire should be inferior compared to that on C-sapphire due to the perturbation of translational symmetry.

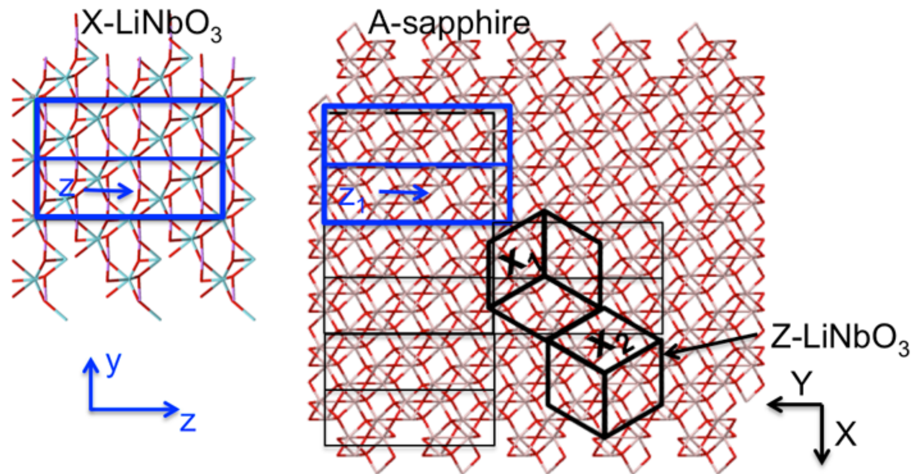

Figure 12. Schematic representation of surface structures and the epitaxial relationships of X-$LiNbO_3$ (or X-$LiTaO_3$) and Z-$LiNbO_3$ (or Z-$LiTaO_3$) grown epitaxially on the surface of A-sapphire substrates. The orientations of the 180 ° growth domains of Z-$LiNbO_3$ are indicated by X_1 and X_2.

Usually, LN films with pure X-orientation on A-sapphire contained two growth domains, rotated in the substrate plane by 76° with respect to each other.[163,200] These growth domains represent X and –X orientations perpendicular to the substrate plane and can be obtained by rotation of 60° around the c-axis.[163] In the case of X and –X domains, the angular arrangement of $(10\bar{1}0)$/ (0001) main planes and higher order $(03\bar{3}6)$, $(03\bar{3}\,12)$, and $(0\bar{6}66)$ family of planes perpendicular to the substrate plane is identical. Therefore the lattice mismatch of these two

growth domains with the A-plane of sapphire is equivalent. It is important to note that the formation of X and –X domains is not related to the ferroelectric domain structure, as both domains may have the same polarization direction. However the in-plane orientation of the lower order planes such as $(01\bar{1}2)$, $(01\bar{1}4)$ and $(0\bar{2}22)$ shows 180 ° symmetry as there is no mirror symmetry in the XY and XZ planes. The major volume fraction of the deposited X-LN films consisted of domains with dense (012) planes aligned to the dense (012) planes of the sapphire substrate as the growth with the same orientation of the dense planes of the film and substrate should be energetically more favourable according to Palatnik's criterion. In the case of LT films, Shibata et al. reported that X-LT films, deposited by PLD on A-sapphire, did not contain growth domains and the LT lattice was perfectly aligned with that of sapphire.[101,138] Unfortunately the authors did not discuss whether the growth domains were eliminated by optimisation of the deposition conditions or if these domains were not observed in general in LT films, which are usually grown at higher temperatures.

As discussed X-axis oriented LN and LT films can be grown on $(11\bar{2}0)$ oriented (hexagonal settings) $LaAlO_3$ substrates which belong to the same space group ($R\bar{3}c$) as sapphire. Better lattice matching can be obtained on $LaAlO_3$ substrates than on sapphire (Table 3). The mismatch between the Y- and Z- axes of LN (LT) and of sapphire are 4.0% (4.0%) and 5.7% (5.0%), respectively.

2.4.3. $(01\bar{1}2)$ ORIENTATION

The $(01\bar{1}2)$ planes in the hexagonal setting are called R-planes (33°Y orientation). High quality epitaxial $(01\bar{1}2)$ LN films were grown on $(01\bar{1}2)$ LT substrates due to the small lattice mismatch.[201] LN films grown on R-sapphire by CVD and ALD methods consisted of a mixture of $(30\bar{3}0)$ and $(01\bar{1}2)$ orientations.[127,131] Dip coating of LN on this substrate resulted in preferentially $(01\bar{1}2)$ oriented films.[132,133] Epitaxial growth of pure $(30\bar{3}0)$ and $(01\bar{1}2)$ out-of-plane orientations of LN/LT on R-sapphire substrates by rf sputtering and PLD has been reported in the literature. The orientation of the deposited LN/LT films on the R-sapphire was highly dependent on the sputtering/PLD deposition conditions. The planes parallel to the film surface were changed gradually from the $(01\bar{1}2)$ to $(11\bar{2}0)$, and finally to $(30\bar{3}0)$ planes by increasing Li/Nb ratio in the target, total deposition pressure, RF power, and oxygen pressure, or by decreasing the deposition temperature. The in-plane lattice parameters of R-sapphire and X-, Y- and 33°Y-LN/LT can be found in Table 3. One can note that the in-plane lattice distance d, of these three orientations are very close ($2*d_{(30-30)}$ is close to the $d_{(01-14)}$). Pure $(11\bar{2}0)$ orientation on R-sapphire substrates and its epitaxial relationship with the substrate surface plane has not been reported in the literature. We can expect that the c-axis of X-LN(LT) is aligned with X-axis of R-sapphire (misfit strain of 2.9% (3.6%)) and five distances between $(30\bar{3}0)$ planes of LN/LT fit to three distances between $(01\bar{1}4)$ planes of R-sapphire with a misfit strain of 8.5%.

In the case of 33°Y oriented layers, $(11\bar{2}0)$ and $(01\bar{1}4)$ planes of LN/LT are parallel to the $(11\bar{2}0)$ and $(01\bar{1}4)$ planes of R-sapphire respectively. The misfits between the planes of the LN (LT) film and the substrate are 8.2 % (8.2 %) and 7.3 % (6.8 %) respectively (Table 3). It is important to note that $(01\bar{1}4)$ planes of LN and sapphire were tilted from the plane by 4.96° and 5.84 ° respectively. The $(01\bar{1}2)$ LN films had two types of growth domains, which were rotated by 180 ° around the surface normal with respect to each other (180° domains, **Figure 13**).[137] In the case of 180° rotated growth domain, X-axis of LN remains aligned to that of sapphire, and the $(03\bar{3}\,18)$ plane is parallel to the $(01\bar{1}4)$ plane of sapphire (misfit strain 7.0%). In this case the dense $(01\bar{1}2)$ planes of LN are not parallel to those of sapphire. Thus we could expect the reproduction of the alignment of the sapphire planes (0° rotated domain) to be more energetically favourable with respect to the film lattice rotated by 180 ° with respect to the substrate lattice. The volume fraction of 180° growth domains was around 20% in $(01\bar{1}2)$ LN films grown on R-sapphire by PLD.[145] Shibata et al. have reported $(01\bar{1}2)$ oriented LT films with single in-plane orientation on R-sapphire grown by PLD.[138]

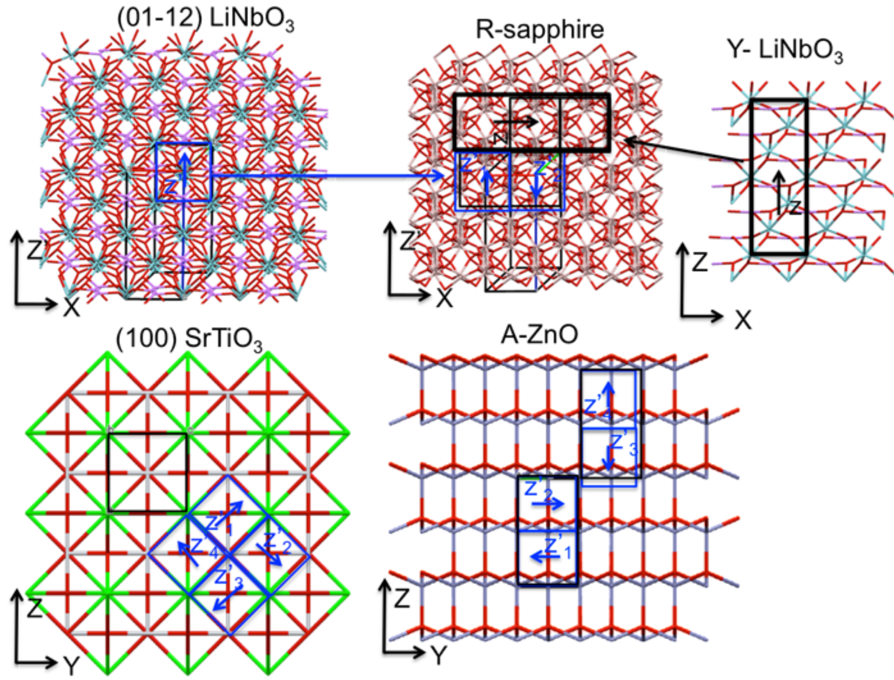

Figure 13. Schematic representation of the surface structures of $(01\bar{1}2)$ $LiNbO_3$ ($LiTaO_3$), R-sapphire, (100) $SrTiO_3$, and A-ZnO. The possible in-plane orientations and the lattice matchings of $(01\bar{1}2)$ orientation of $LiNbO_3$ ($LiTaO_3$) on these substrates. Note that Z' indicates the projection of the Z+ axis to the substrate plane. The epitaxial relationship of Y-LN with R-sapphire is illustrated, as well.

It was reported that A-ZnO layers can be grown epitaxially on R-sapphire substrates. Knowing that in-plane parameters of A-ZnO are better matched to the $(01\bar{1}2)$ LN lattice than that of R-sapphire ($(11\bar{2}0)||(0002)$, Table 3) we can expect epitaxial growth of $(01\bar{1}2)$ LN layers on A-ZnO buffer layers or single crystals. 180 ° domain structure can be expected, as the rotation in plane by 90° would introduce a much higher lattice mismatch (Figure 13). It was identified that $(01\bar{1}2)$ oriented LN films can be grown epitaxially on (pseudo-) cubic substrates or buffer layers with the in-plane lattice parameters close to 0.26 nm. The $(01\bar{1}2)$ orientation of $LaAlO_3$ in hexagonal settings is represented by the (100) orientation in the cubic setting. The interplanar distance between $(01\bar{1}2)$ planes is 0.3791 nm (cubic cell parameter). LN layers with a mixture of $(30\bar{3}0)$ and $(01\bar{1}2)$ out-of-plane orientations were also obtained on $(01\bar{1}2)$ $LaAlO_3$ substrates by ALD.[131] 33°Y $LiNbO_3$ layers with single out-of-plane orientation were successfully grown on $(01\bar{1}2)$ $LaAlO_3$ by PLD[145] and MOCVD. The distortion of the four-fold symmetry of the $(01\bar{1}2)$ plane is small and the surface plane looks more like a (100) cubic than the $(01\bar{1}2)$ plane in the hexagonal cell of rhombohedral structure. Therefore 33°YLN films on LAO substrates usually present growth domains with four different in-plane orientations, rotated by 90° around the surface normal. The epitaxial in-plane relationships between 33°Y-LN/33°Y-$LaAlO_3$ are $X_{LN}||X_{LAO}$, $X_{LN}||-X_{LAO}$, $X_{LN}||(01\bar{1}\bar{4})_{LAO}$, and $-X_{LN}||(01\bar{1}\bar{4})_{LAO}$. Consequently, 33°Y-LN/LT films can be grown on other (100) oriented cubic substrates and layers ($SrTiO_3$, LSAT, Pt, MgO, GaAs, Y_2O_3, etc., see Table 3). Only a few of these materials have been tested for epitaxial growth of LN/LT films.[131,195,202] It is important to note that the default in-plane orientation of 33°YLN layers on (100) cubic substrates/layers would always be represented by at least four growth domains rotated by 90° in the surface plane due to four-fold symmetry of the substrate. Growth domains with four orientations of the c-axis projection rotated relative to each other by 90° in the substrate plane were observed in epitaxial growth of LN on (100) cubic $SrTiO_3$ substrates (Figure 13). In these four crystallographic orientations the X-axis of LN was parallel to the (011), $(0\bar{1}1)$, $(0\bar{1}\bar{1})$, and $(01\bar{1})$ axis of $SrTiO_3$. Films with two growth domains could be obtained on tetragonal (with c-axis not parallel to the surface normal) and orthorhombic substrates. The growth of $(01\bar{1}2)$ LN films on (110) orthorhombic $NdGaO_3$ (NGO) substrates was reported.[195] These films consisted of two growth domains, in which the X-axis and $(01\bar{1}\bar{4})$ axis of LN are

exchanged. These LN planes were aligned with the $(1\bar{1}\bar{2})$ and $(1\bar{1}2)$ planes of NGO. A tilt of the LN unit cell from the substrate surface plane by 4.6° was observed, which can be explained by the perfect match of the $(01\bar{1}\bar{4})$ LN plane on the $(1\bar{1}\bar{2})$ NGO plane (misfit strain of 0.2%).[195] As mentioned above, the $(01\bar{1}\bar{4})$ plane is tilted by 4.96° from the surface plane in the $(01\bar{1}2)$ oriented LN. To match the $(01\bar{1}\bar{4})$ plane on the $(1\bar{1}\bar{2})$ $NdGaO_3$ plane, the $(1\bar{1}2)$ LN axis is tilted from the surface normal by around 5° by keeping the X-axis of LN parallel to the surface plane. Epitaxial growth of $(01\bar{1}2)$ LN has also been achieved on a c-axis oriented orthorhombic $YBa_2Cu_3O_{7-\gamma}$ superconducting electrode on a (100) $SrTiO_3$ substrate.[203] Preferential $(01\bar{1}2)$ texture of LN layers was obtained on (002) quartz[150,204,205] and (111) diamond.[206]

2.4.4. $(10\bar{1}0)$ ORIENTATION

The $(10\bar{1}0)$ planes in the hexagonal setting are labelled the M-planes. The axis perpendicular to the $(10\bar{1}0)$ planes is called the Y-axis. Two co-existing epitaxial in-plane relationships of Y-LN(LT) layers with the R-sapphire substrate are [0001]LN‖$[2\bar{1}\bar{1}0]$saph and $[000\bar{1}]$LN ‖$[2\bar{1}\bar{1}0]$saph[137] with a misfit strain of 2.9% (3.6%) (Figure 13, Table 3). The matching between $(11\bar{2}0)$ planes of LN(LT) and (0114) planes of sapphire is very good (misfit strain of 1%). It was calculated theoretically, by using Coulomb's law and a rigid lattice approximation, that the cohesion energy Y-LN/R-sapphire is higher than that of 33°Y-LN/R-sapphire, which is also related to the lower mismatch of the hetero-structure.

The change of epitaxial orientation with deposition conditions can be explained by a similar mechanism as for the Z- and X-LN growth on the A-sapphire (see above). The mismatch between the unit cell of LN (LT) and R-sapphire decreases from $(01\bar{1}2)$ to $(11\bar{2}0)$, and the best matching is with the $(10\bar{1}0)$ orientation. The translational symmetries of the $(11\bar{2}0)$ and $(30\bar{3}0)$ orientations are not the same as that of the $(01\bar{1}2)$ orientation. Although the misfit between lattices is considerable, at high adatom energies and mobility the layer will adopt the long range structure of the surface of the substrate. The layer will adopt the best fitting local structure (at the unit cell level) when the mobility of adatoms is limited (low adatom energies at low deposition temperature, high pressure, etc.).

The growth of Y-axis oriented LN films was obtained also on the $(11\bar{2}0)_{AlN}/(01\bar{1}2)_{sapphire}$[138] and $(0002)_{Al:ZnO}/(0001)_{quartz}$.[61] Their structure and epitaxial quality have not been studied. Thus, it remains unclear why growth along the Y-axis was favoured and not the well-matching $(01\bar{1}2)$ orientation of LN films on the $(11\bar{2}0)$ AlN buffer layer (Table 3). The growth of Y-LN on a C-ZnO layer is surprising, as c-axis oriented ZnO films are usually grown on Z-LN substrates [207] and epitaxial Z-LN growth on an (0002) ZnO crystal was reported.[185] In order to favour the Y-orientation of LN/LT layers on R-sapphire, the use of an intermediate layer was proposed (Nb_2O_5, Nb, Ta_2O_5, Ta, Al_2O_3, Al, etc.) with thickness of 0.5-3 nm, which is absorbed during the LN/LT growth and serves to homogenize the surface chemical state.[208] Y-LN layers were epitaxially grown on M-sapphire substrates by MOCVD. Most of the grown layers consisted of four growth domains with $(30\bar{3}0)_{LN}$‖$(30\bar{3}0)_{Saph}$ rotated by 90° in the substrate plane: (i) $[0001]_{LN}$‖ $[0001]_{Saph}$; (ii) $[0001]_{LN}$‖ $[\bar{1}\bar{1}20]_{Saph}$; (iii) $[000\bar{1}]_{LN}$‖$[0001]_{Saph}$; (iv) $[0001]_{LN}$‖ $[11\bar{2}0]_{Saph}$ (**Figure 14**). The main volume fraction consisted of Y and –Y domains (rotated by 60° around the c-axis) with $(0001)_{LN}$‖$(11\bar{2}0)_{Saph}$. It was possible to obtain Y-LN films with a single orientation on M-sapphire ($(30\bar{3}0)_{LN}$‖$(30\bar{3}0)_{Saph}$ and $(0001)_{LN}$‖$(0001)_{Saph}$) by significantly reducing the growth rate. The Y-cut of $LaAlO_3$ substrates should also be suitable for the epitaxial growth of Y-LN/LT films, as the lattice of Y-LN fits even better to the Y-$LaAlO_3$ lattice than that of M-sapphire. $(10\bar{1}0)$ ZnO films were grown on Y-cut LN substrates.[209] The epitaxial growth of Y-LN/LT films on $(10\bar{1}0)$ ZnO crystal or buffer layers should also be possible (Figure 14, Table 3). Although the epitaxial relationship between Y-LN and ZnO was not studied in detail, the formation of two – four orientations of growth domains can be expected: 180° domains or 90° domains. In a similar way, Y-LN/LT films can be grown on other hexagonal crystals/buffer layers, such as AlN and GaN, with in-plane lattice parameters close to those of ZnO (Table 3).

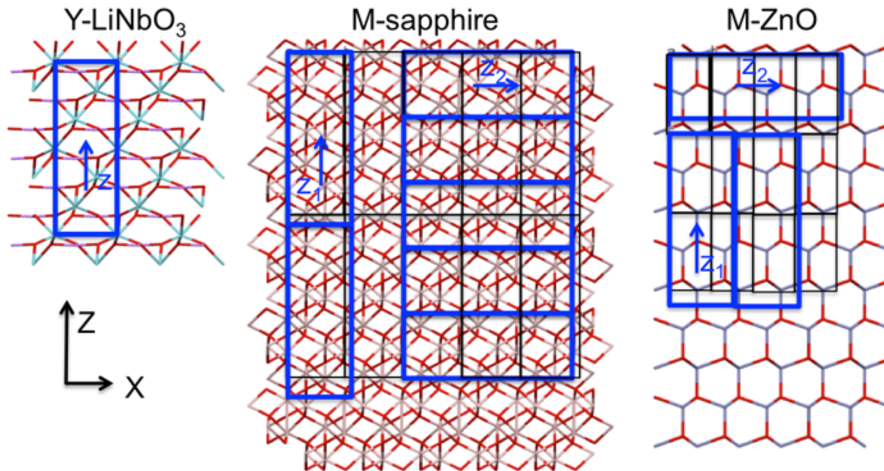

Figure 14. Schematic representation of the surface structures of (30$\bar{3}$0) planes (or Y-cut) of $LiNbO_3$ ($LiTaO_3$), M-sapphire, and M-ZnO and possible in-plane orientations and the lattice matchings of Y-orientation of $LiNbO_3$ ($LiTaO_3$) on these substrates are shown.

2.4.5. INTEGRATION WITH SILICON TECHNOLOGY

The integration of LN and LT films with silicon technology has several advantages. Development of next generation of multifunctional devices and their miniaturization would be possible through co-integration of electro-optic, acoustic, pyroelectric, energy harvesting devices or active micro-electronic components. Si is used as a bottom electrode and SiO_2 with low refractive index as a base for waveguiding layer or cladding layer. So SiO_2/Si wafers have potential for the exploitation of electro-optic properties and waveguiding simultaneously. As mentioned above, the replacement of AlN films in TFBAR and SMR structures, would allow progress to the next generation of wide-band high-frequency or tuneable acoustic filters by using a standard and robust Si microfabrication technology. Simple deposition of LN and LT layers on Si platforms would be a much cheaper alternative to complex bonding processes. The frequency of the BAW is directly defined by the piezoelectric film thickness, therefore the precise control of the thickness is a key issue in TFBAR and SMR device fabrication. The best control of the film thickness (reproducibility and the lateral homogeneity over large surfaces) is offered by chemical deposition methods. Thickness variations in the order of 1% can be obtained by CVD/ALD techniques, such precision is a huge challenge in the methods based on ion-slicing or polishing LN/LT single crystals. This strongly encourages the studies on LN/LT growth on Si and at present the Si substrate is the most frequently used substrate for these films in the literature.

The (111) and (100) planes of Si match quite well with the (0001) and (01$\bar{1}$2) orientations of LN and LT (see Table 3), respectively. The misfit strain of LN (01$\bar{1}$4) planes on (020) planes would be only 0.7% in the case of (01$\bar{1}$2)LN/(100)Si and a misfit strain of 3.3%-5% (4*d(30$\bar{3}$0)LN on 3*d(2$\bar{2}$0)Si and 2*d(11$\bar{2}$0)LN on (d(22$\bar{4}$)Si, respectively) would be present during the nucleation of Z-LN on (111)Si. The direct epitaxial growth of LN/LT on Si has never been reported due to the formation of a native amorphous SiO_2 layer on the Si surface and the SiO_2/Si chemical interaction with LN and LT at high deposition temperatures. The temperature at which the chemical interaction between the LN/LT film and the SiO_2/Si substrate begins depends on the deposition method. Sharp interfaces between SiO_2 and LN were obtained by means of PLD at deposition temperatures of 600–720°C.[210-213] For rf sputtering the SiO_2 interacted with LN at temperatures higher than 450-500°C, while the formation of silicates was not observed at the interface between the Si and LN layer, grown at 530°C.[134,214] It was shown that the presence of plasma accelerated the interaction between SiO_2 and LN.[134] A thick silicate interlayer was observed in LT/LN films grown at 575°C by thermal plasma spray CVD.[215] This indicated that the SiO_2 and LN/LT interaction can be enhanced by the presence of the plasma or the reactive environment such as in CVD processes. The presence of silicates at the interface

decreased the growth of the preferential c-axis orientation and resulted in polycrystalline films. It is important to note that most of the publications have reported polycrystalline LN/LT films with preferred orientations on (SiO_2)/Si substrates and on hetero-structures consisting of buffer or electrode layers on Si. These works will not be discussed in this paper as polycrystalline films of LN/LT do not present any real potential for industrial applications. A particular effort has been made to obtain c-axis textured LN/LT films on Si based hetero-structures and substrates.

To obtain c-axis textured LN films on Si substrates different approaches have been used. The growth of LN and LT films with pure c-axis texture were grown at optimised conditions by PLD,[154,210,211,216,217] rf sputtering,[134,165,218,219] sol-gel[220] and CVD.[215,221] The film texture on SiO_2/Si largely depended on the deposition temperature.[215,217,222] The deposition temperature of LN/LT films with a single texture was in the range 530-720°C. The possibility of growing c-axis textured films on amorphous surface layers originates from the anisotropy in growth rate along different crystallographic axes in LN and LT. The growth along the c-axis was favoured by deposition conditions resulting in the reduced mobility of ad-atoms (for example at increased deposition rate, relatively low deposition temperatures, sufficiently high oxygen pressure, etc.).[215,217,223] This approach was also to obtain c-axis oriented LN films on nano-crystalline diamond substrates with a SiO_2 buffer layer by PLD.[224,225] An amorphous Al_2O_3 or Si_3N_4 layer on SiO_2/Si was also an efficient way to initiate c-axis texture of LN films, grown by PLD and rf sputtering, respectively.[226-228] To obtain c-axis oriented LN films, Akazawa et al. have suggested a solid-phase crystallization from the surface to the interface by rapid thermal annealing of amorphous LN/LT films on amorphous TiN buffer layers with higher crystallization temperatures than those of LN and LT.[218] If the buffer layer is polycrystalline or crystallizes at lower temperatures than LN/LT, it serves as a crystallization seed and purely c-axis oriented films cannot be grown or crystallized.[218] The smooth surface of the amorphous layer during deposition or crystallization of the layer is a key factor determining the quality of the texture.[216,218] A similar approach, used in the literature for the growth of Z-LN/LT on Si substrates, consists of growing of a buffer layer with a lattice matching to the LN/LT lattice and with a highly anisotropic growth rate such as (002) ZnO,[148,182,184,190,229] (111) Pt, (111)MgO,[230] etc. An original approach used to obtain C-LN/LT films on Si is the application of an *in-situ* electric field of 7-8 V/cm during PLD, which forced the texture along the polarization axis, as the growing LN layers were ferroelectric at deposition temperature.[222,231,232] Textured LN/LT films, without defined in-plane orientation, are not suitable for applications requiring a defined propagation direction and single-mode responses as SAW, Lamb wave and optical applications. Highly defective grain boundaries in textured films introduce significant acoustic and optical propagation losses. Nevertheless textured films can be used for energy harvesting, BAW (TBAR and SMR devices), and pyroelectric applications. It is worth noting that the Z-axis oriented LN and LT have similar electromechanical coupling to the AlN layers, produced already at industrial level on Si substrates) in TFBAR and SMR. The figure of merit of energy harvesters based on C-LN films cannot be competitive with those based on PZT or other lead-free materials.[139,233]

Only a few reports can be found on the epitaxial growth of C-LN/LT films on Si and the possibility of obtaining textures or epitaxial growth with orientations (oblique orientation of polarization axis) having higher electromechanical coupling. Joshi et al.[234] and Huang et al.[235] have produced preferentially ($01\bar{1}4$) oriented LN films by low-temperature sol-gel derived growth on Si(100). Tao et al. reported a preferential ($01\bar{1}2$) texture of LT films grown by MBE on epitaxial (100)PtSi/(111)Si hetero-structure[151] (see Table 3 for the possible epitaxial relationship between (100)Pt and ($01\bar{1}2$) LT). The epitaxial growth of these orientations was not reported and the growth mechanisms of these orientations remain unclear.

Epitaxial hetero-structures of Z-LN/LT (or other ferroelectric films) on epitaxial buffer layers (111)MgO or $MgAl_2O_4$ on (111)Si substrates (similar to the Z-LN/(111)MgO/(111)GaAs heterostructure described above) were patented by Nashimoto et al.[230] Epitaxial (111) oriented Y_2O_3 epitaxial layers were grown on (111) Si substrates[236] The in-plane lattice parameters of (111) Si and (111) Y_2O_3 can be found in Table 3. The Y_2O_3 films on (111) Si contained single in plane orientation. (0001) LN layers were grown epitaxially on this Y_2O_3/Si heterostructure.[236]

The LN films had a reasonable texture (the FWHM of the (0006) rocking curve was 0.77°), defined orientation in the substrate plane and had 180° growth domain structure.

2.5. SURFACE MORPHOLOGY AND ROUGHNESS

The surface morphology and roughness of the films are one of the key factors determining the optical and acoustic performances of devices. Optical and acoustic attenuation results from the scattering from inhomogeneities, impurities, twins, grain boundaries or rough surfaces.[135] For optical and acoustic applications, LN and LT films with surface roughness of around 1 nm are required. The presence of particles on the surface causes strong light scattering. Therefore for MOCVD, very high deposition temperatures and low temperature gradients in the proximity of the substrate holder and other deposition conditions favouring decomposition of the precursors in the volume are not recommended. To eliminate the particles arriving on the film surface during the PLD process, a shadow mask was used.[161]

The growth of thin films comprises several steps: physical, chemical or dissociative absorption of molecules/atoms on the surface (and desorption of reaction products in chemical processes), surface diffusion, nucleation and layer growth. The atoms or molecules absorbed on defect sites or in contact with other layer atoms are immobile. LN films on LT substrates had a much smoother surfaces than the sapphire substrates due to the lower lattice mismatch.[116] The surface morphology and roughness of grown films are also highly dependent on the film orientation, as the growth rates along different crystallographic axes differ[187] and nucleation mechanisms are not the same. The large mismatch between film and substrate lattices strongly affects the crystalline quality of the layers and the surface roughness. When nuclei grow on the surface with a large surface mismatch, the growth along the interface is less favourable than the growth on the film surface. This favours Volmer-Weber (three-dimensional island growth mode) or Stranski-Kraustanov growth mechanisms but not two-dimensional layer by layer growth.[135] The island shape and height highly depends on the crystallographic orientation due to anisotropy in the growth rate. In the case of C-LN films the islands have a triangular-pyramid-like shape in the epitaxial growth conditions[116,135,180] and dome-like shaped islands formed in the polycrystalline/amorphous films[125] (**Figure 15**). No specific shape of nuclei was reported for the X- or Y-LN(LT) films. At higher nuclei densities, the islands of X-LN tend to arrange in lines on A-sapphire.[237] The coalescence of the islands results in the formation of the defective grain boundaries and grain boundary grooves, which contributes to the surface roughness. The surface roughness is directly related to the island size and shape. At low deposition temperatures (around 500°C), the adatom mobility is low and the surface roughness of as-grown LN/LT films at low temperatures is rough, due to low mobility, poor epitaxial quality, the growth of the island height is preferred to lateral growth, this induces formation of deep groves and high roughness[135] (Figure 15). When the growth temperature is increased the lateral growth rate is accelerated and the islands are much flatter and the resulting morphology is smoother (Figure 15). A further increase of temperature resulted in the increase of roughness as the lateral island and valley dimensions started to increase. The film roughness, RMS, is proportional to the square of the lateral diameter of the islands, r, $RMS = \frac{r^2}{2h}$, where h is the film thickness.[135] It was found that the small grain size at the nucleation stage resulted in the smooth surfaces. The nuclei critical size depends on the bonding energy, precursor flux, energy of diffusion (depends on the surface, its quality and the strength of bonds substrate-film). The crystallite size depends on the nucleation density and the size of nuclei is limited at high nucleation densities.[135] The nucleation density, J, is described by $J = AP_i^2 \exp\left(-\frac{\Delta G}{RT}\right)$, where P_i, the precursor partial pressure, A, a constant, ΔG, the activation energy for nucleation, T, the growth temperature.

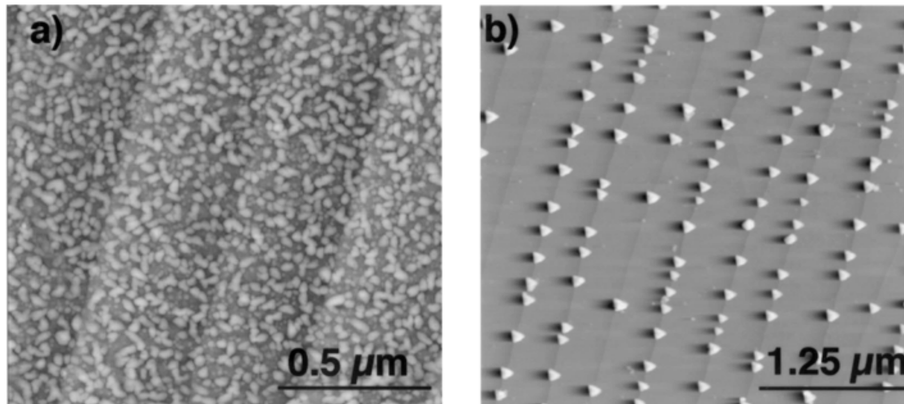

Figure 15. Nucleation of C-$LiNbO_3$ film on the annealed C-sapphire substrate at 550°C (a) and 675°C (b).
Reproduced with permission. [135] Copyright 1998, Elsevier.

The primary factor determining the nucleation density is the surface quality of the substrate. The surface of as-received wafers contains polishing defects such as hillocks and scratches. Several research groups studied the possibility of ameliorating the surface quality of the wafers by annealing in air at high temperature.[116,135,237,238] For sapphire, an annealing temperature of 1000-1500°C was used. The surface during the annealing « self-heals » the crystalline structure of the surface and forms a smooth surface with steps with reduced total energy of the surface. The height and the number of the steps can be modified by changing the annealing temperature, duration and the angle of the vicinal cut.[135,238] The un-treated surfaces contained a large number of surface defects which served as nucleation sites. For restructured surfaces the nucleation sites can be limited to the surface step edges if the height of the step is higher than that of the growth unit (the smallest unit which satisfies charge neutrality and the chemical composition).[163] The height of the growth unit in X-LN and R-LN is around 0.3 nm and in Z-LN- 0.67 nm.[163] The nucleation density can also be increased by reducing the mobility of adatoms (decreasing the deposition temperature or increasing the growth rate). However, at low temperatures and high deposition rates the crystalline quality of grown layers is poor. Therefore, two-step processes were proposed: the initial step is carried out with high nucleation density and then the further growth is continued at lower deposition rates and/or higher temperatures to ensure high crystalline quality. This approach was adapted for the growth of LN/LT layers by means of CVD[124,135] and PLD processes[200] and the surface roughness of grown layers was reduced by several times.

2.6. Residual stresses and relaxation mechanisms

Stresses and clamping effect in films can considerably change the structural, optical, mechanical, piezoelectric, and electrical properties, which play an important role in the device performance and reliability.[239-241] The clamping of the film structure by the substrate can be illustrated by the temperature evolution of lattice parameters of epitaxial LN and LT films on sapphire.[146] The films relax the residual stresses relatively quickly with the increase of the film thickness, but the clamping effect diminishes very slowly with film thickness and remains relatively large even in relaxed and cracked films.[153] Epitaxial LN and LT films were grown on the substrates with relatively large lattice mismatch, as described above (Table 3). The high misfit strain greatly affects the nucleation mechanism and the crystalline quality of the layers. The relaxation of high misfit stresses by the formation of misfit dislocations at the strained interface in the first atomic layers was confirmed by detailed TEM analysis.[122,242] The misfit strain in X-LT films on A-sapphire was accommodated by the creation of two sets of orthogonal sets of noninteracting dislocations with two different Burgers vectors ($1/3(1\bar{1}00)$ and $1/3(0001)$).[122] The misfit dislocations were equally spaced along the C- and a-axis.[122,155] In the case of C-LN/C-sapphire, the misfit strain relaxation took place over two or three lattice planes and the Burgers vector was $½(10\bar{1}0$.[242] The spacing between dislocations in X- and Z-LN films

confirmed that the misfit strain was released completely and the films were in a stress-free state during growth.

Many publications reported high thermal stresses and cracking in epitaxial LN/LT films, but little is known about the stress effect on the physical and structural properties of such films.[95,146,243] LN and LT have very high thermal expansion along the a-axis and the commonly used substrates for the growth of LN/LT films have thermal expansion several times lower than that of LN/LT (**Table 4**). Therefore epitaxial LN/LT films with X- and/or Y-axis in the substrate plane are subject to high thermal tensile stresses (on the order of 1-2 GPa). Unfortunately, in all the LN/LT orientations studied (summarized in Table 3) at least one of these axes is in the substrate plane. The smallest thermal stresses would be induced by the LT/LN and MgO substrates. When critical thickness is reached, cracks and elastic twins form in the layers to release the high thermal stresses. The cracks and twins induce high acoustic and optical losses and contribute to the degradation of the physical properties. The relaxation mechanism through the formation of cracks and twins is very well known in single crystals of LN and LT under compositional and/or thermal stresses. The elastic twins and cracks form along the dense – cleavage $(01\bar{1}2)$, $(1\bar{1}02)$, $(\bar{1}012)$ planes of the LN/LT structure.[26,244-248] The c-axis, responsible for the spontaneous polarization, is tilted out of normal to the substrate surface in the $(01\bar{1}2)$ twins. Thus the twin structure reduces the spontaneous polarization of the film and induces optical losses due to light scattering. The presence of 180° domains may reduce the spontaneous polarization due to pinning of the domain walls by defects.[249] Twins and cracks form simultaneously and a twin plane can be replaced by a crack plane and vice versa.[247,248] Although cracking of the epitaxial films has been a major problem since early work on LN/LT films, very few reports exist on the elastic twinning in the layers. The relaxation of thermal stresses in LN films by the formation of elastic twins with mirror symmetry relative to the $(01\bar{1}2)$ plane was confirmed by TEM analysis,[242] XRD, and Raman spectroscopy.[129] The stereographic projections representing the in-plane and out-of-plane orientations of the c-axis oriented LN matrix and the three twin components are given in **Figure 16**. These types of twins have also been observed in LT layers on C-sapphire.[121] Twins with lamellae-shape were inserted in the film matrix and were in contact with the cracks.[242] This confirms that the creation of the cracks is closely related to the twining. It was observed that 270-500 nm thick C-LN films deposited at relatively low temperature (650°C) did not contain twins, although, a 500 nm thick film was cracked. During heating to higher temperatures (850°C), the energetically less favourable 180° growth domains were eliminated but stress relaxation was activated by the formation of elastic twins.[129] The twins can be represented with a quite low volume fraction (5-10%). Nevertheless, this twin structure may induce significant optical and acoustic losses due to light scattering.

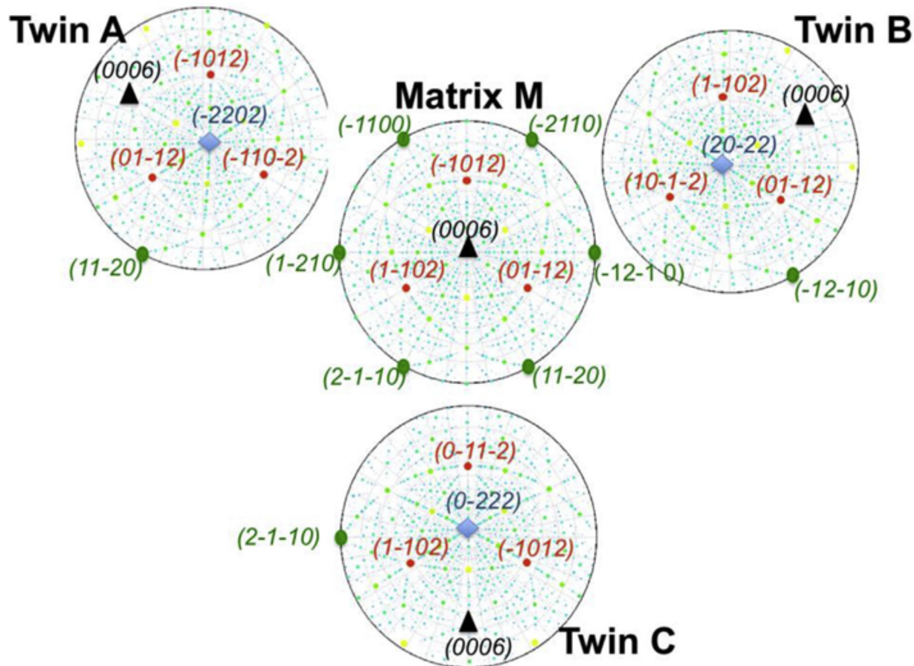

Figure 16. Steoreographic projections representing orientation with respect to the surface normal of three out-of-plane {$\bar{1}$012} family twin components (named A, B and C) and the matrix of C-$LiNbO_3$ film (M).
Reproduced with permission. [129] Copyright 2015, Elsevier.

Large thermal stresses limit the maximum thickness which can be achieved for crack-free films. This limit to the film thickness strongly depends on growth conditions such as deposition temperature, temperature gradients, cooling rate, and the crystalline quality and compositional/orientation homogeneity of the film. No thickness limitation was observed for LN/LT films grown on LN/LT substrates due to very similar lattice and thermal expansion coefficients. However, it is important to note that very thick X-axis oriented LN films on X-LT substrates grown by LPE showed cracks due to difference in thermal expansion of c-axis of LN and LT. Usually, Z-LN/LT films on C-sapphire with thicknesses higher than 500 nm contained cracks. However, in some cases (nano) cracks were observed in Z-LN films at thicknesses as low as 100-200 nm.[242] The possibility of growing crack-free thick (01$\bar{1}$2) LN/LT (thickness much higher than 500 nm) on R-sapphire due to small thermal stresses was claimed by Shibata et al.[208] However the greatest thickness of LT on R-sapphire reported by these authors is 560 nm. In the case of (01$\bar{1}$2) LN/R-sapphire the thermal stresses are much lower along the (01$\bar{1}$4) axis of LN, but the X-axis is still subject to very high thermal stresses on R-sapphire (Table 4). A similar stress-state is present in the X- and Y-oriented LN/LT films. It was observed that such almost uniaxial stress is usually relaxed by the formation of the cracks perpendicular to the direction of high tensile thermal stresses. Growing thick LN films by a multistep deposition process was suggested, whereby during each step the deposited layer thickness is lower than the critical thickness for crack propagation.[158]

3. Physical properties and targeted applications

3.1 Ferroelectric domain structure

LN and LT are ferroelectric materials and to preserve the high electromechanical coupling and electro-optic effect in these films they need to be electrically poled. This procedure is not needed for the non-ferroelectric piezoelectric AlN films and this has facilitated its integration into industrial processing. This step is likely to be the major difficulty in the case of LN and LT films, because the grown films are usually polydomain.[116,145,250,251]

Different methods have been used to characterize the ferroelectric domain structure in the LN and LT films: scanning non-linear dielectric microscope,[83] piezoelectric force microscopy (PFM),[251,252] electrostatic force microscopy (EFM),[145,253] pyroelectric current measurements,[109] confocal second harmonic microscopy,[254] and selective chemical etching by HF solutions.[168,255] It was suggested, that the grains with Z- orientation grow much faster than Z+ grains during rf sputtering[255] However selective etching by HF (Z- domains are etched faster than Z+ domains) is not sufficient to confirm that the outgrowths had opposite polarity and they were not parasitic phases or an inhomogeneity of Li concentration. The etching rate is highly dependent on doping and Li non-stoichiometry of the $LiNbO_3$ phase and it differs for different crystalline phases. Further experiments, such as PFM (piezoelectric force microscopy) characterization, separating the topography from the polarity and identifying the polarity sign are necessary to confirm this. Some authors have wrongly believed that the presence of the SAW signal confirms the single domain state of the layer. A ferroelectric polydomain structure does not destroy the piezoelectricity of the material, but reduces the electromechanical coupling (K^2 is low but not zero)[256] and induces propagation/insertion losses. SAW waves can be generated on polydomain samples and periodically poled structures.[257]

In some cases it was found that most of the polarization domains aligned by themselves in c-axis oriented LN films on sapphire deposited by sputtering and PLD.[161,255] It was suggested that the Z+ domain was slightly energetically favourable than Z- domain due to better atom stacking on the C-sapphire surface. This self-poling effect was not observed in C-LN films grown on C-sapphire by chemical methods. Thus the origin of this effect remains unclear taking into account that other papers published a polydomain state in the films grown by PLD and sputtering methods.[145,252] A single domain state of the grown material can be achieved in the presence of thermoelectric fields generated by the steep temperature gradients across the material (observed in LN fibre growth).[258] It is believed that the compositional gradient also generates the internal electric field due to the difference in polarization of the ferroelectric film and the ferroelectric substrate.[259,260] These internal fields may induce the growth of Z- or Z+ self-poled films on ferroelectric substrates such as LN and LT. It is important to note that the sign of the polarization axis was independent of the polarity of the substrate but it was greatly affected by the Li composition of the film.[116] The self-polling effect appeared only in the films grown at temperatures below the Curie temperature. Although the polarity of the films might be forced by the internal fields, these fields might be modified locally by the grain boundaries and other defects, which may induce the residual fraction of ferroelectric domains with opposite polarity in the films in an irreproducible manner.[189] Moreover commonly used sapphire, Si and other substrates are not polar and the films usually grown are polydomain.

The most common poling technique used in industry for the grown poly-domain crystals and films is ex-situ electrical poling. In this case the electric field applied has to be higher than the electric coercive field, E_c, of the crystal. For LN, the coercive field increases several times with the decrease of Li_2O concentration by 1 mol%.[14] To facilitate domain reversal, crystals/films with applied electrodes can be heated above Tc and then the electric field is applied during the cooling from temperatures higher than Curie temperature to room temperature. In general the coercive fields are small in proximity to the Curie temperature and thus small electric fields are sufficient to orient domains uniformly.[261] At room temperature homogeneous electrical poling of polydomain crystals and films is complicated and usually not efficient due to the presence of internal screening fields on the domain walls, and low mobility of ions and domain wall pinning on the defects.[262] In the case of polydomain films high-temperature poling has to be considered. The major complicating factor in the case of LN/LT films is that they are usually grown on dielectric substrates or buffer layers for waveguiding and SAW applications. An In-situ electric field was applied during LN film deposition to favour the growth along the polarization axis on Si, SiO_2/Si and sapphire by PLD and rf sputtering.[231,232,263] c-axis texture could not be achieved in the LT films on fused silica by this method.[264] This probably could be explained by the Curie temperature of the layer being below the deposition temperature of 600°C. In-situ electric field induced preferential growth along the c-axis and stronger electric fields were needed to initiate such growth on dielectric substrates or buffer

layers. Unfortunately, the ferroelectric domain structure was not studied of these films. It is not known if this method is efficient for the growth of single-domain films on dielectric substrates, such as sapphire. It would be difficult to adapt this method for films with an in-plane polarization direction. Therefore, electrical poling techniques adopted for the thin film technologies have to be developed to obtain single-domain films and to create a periodic well-controlled domain structures for quasi phase matching and nonlinear integrated circuits. Recently it was demonstrated that it was possible to pole X-cut LN film on an SiO_2/LN substrate (obtained by smart-cut technology) by using periodic electrodes with a gap along the Z-axis on the top of the layer.[254] The possibility to invert the domain polarity locally in polycrystalline LN films on SiO_2/Si, Pt/Si, Si and ITO/Si substrates by means of PFM and EFM was (**Figure 17** demonstrated).[251-253] During the last decade, the understanding and control of domain inversion in Z-, X- and Y-cut LN single crystals and single crystalline films by focused ion beam and e-beam writing advanced significantly[265-268] and probably these methods will be applied to deposited films in the near future.

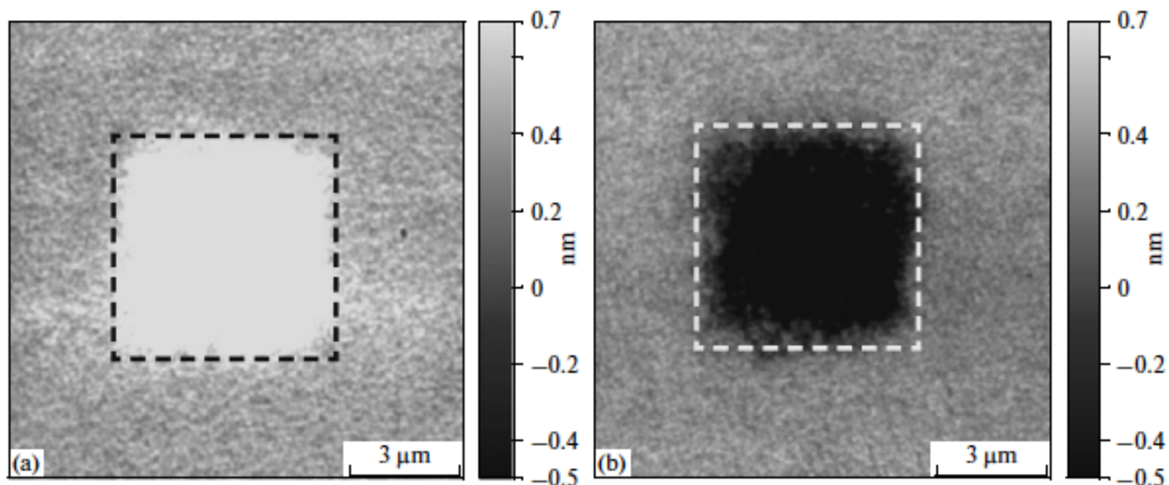

Figure 17. Residual signal of piezoresponse of $LiNbO_3/SiO_2/Si$ film after poling of the highlighted square by a constant voltage of +20 V (a) and -20 V (b).
Reproduced with permission. [252] Copyright 2012, Pleiades Publishing.

3.2. Optical properties and devices

The use of deposited LN and LT films in guided photonic applications remains very challenging. In theory, the creation of a high index-contrast in thin films should be straightforward by growing the film on a substrate that has a lower refractive index than LN. However, the refractive indices of LN and LT films depend on various compositional and structural parameters (**Table 5**). For example, a change in the Li/Nb ratio by 5 % modifies the refractive index of the extraordinary axis.[20] The refractive index of amorphous films drops to a value of 2.1 (electro-optic effect disappears).[60] The effects of the substrate clamping and the residual stresses on the refractive index (related through the photoelastic effect) and on the polarizability have not been considered extensively in the literature.[269] The refractive index of thin films might be different from that of bulk LN and be dependent on the film composition, crystalline quality and residual stresses. This explains why LN films grown on LT substrates, which have a small difference in refractive index were frequently not guiding or had high losses (8 dB/cm in the visible[116]). Therefore, in waveguiding applications, fine control of stoichiometry and stresses in thin films is of key importance. Lower losses were measured in LN/LT films on a sapphire substrate (offering higher refractive index contrast). To ensure correct mode propagation the guides need to be uniform in thickness over the full propagation length. This point has not been systematically studied in the literature. Thus propagation losses better than 0.5 dB/cm in the visible range (λ=633 nm) for $LiNbO_3$ or $LiTaO_3$ thin films on different substrates have never been published.

Losses are another limiting parameter related to the quality of the crystals and films. For bulk single crystals, losses in as grown crystals are attributed to the compositional inhomogeneity, twining, dislocations, ferroelectric polydomains, etc.[270,271] Oxygen vacancies (reduced or 'black' crystals) affect the absorption.[272] However, these losses can be significantly reduced using the high temperature oxygen annealing and poling.[273] Other losses have been attributed to the photorefractive effect and damage under a high incident flux due to iron impurities.[274] Nearly stoichiometric crystals have a low threshold. The losses can be limited by using extra-pure raw materials or by introducing damage resistant dopants such as Mg. For the thin films, losses by absorption are generally not considered in the literature. Excluding contamination that can occur by processing outside clean room facilities, one must pay attention to absorption related to oxygen vacancies as thin films grown in vacuum conditions are "grey". Such films have reduced oxygen stoichiometry and some residual conductivity.[275] In principle, annealing in an oxygen environment should eliminate this problem, leaving dielectric losses as the limiting factor. The dielectric losses can be classified into two categories:[276]

- Losses due to scattering in the volume of the guide. These losses occur due to dielectric fluctuations in the scale of the order of the wavelength and are wavelength dependant. They may originate from interfaces (grain size, dislocations), structure defects (texture, twins), homogeneity (partly crystallized films, piezoelastic fluctuations, parasitic phases) and stress gradients in epitaxial films. One may note that ferroelectric domains are considered not to affect the linear index, but single domain films should be preferred for electro-optic applications. [264 Moreover, transforming amorphous films into polycrystalline films by thermal treatment results in high losses due to birefringence.[60] Thus, lower losses are expected for epitaxial layers. However, epitaxial films of LN grown on (0001)-sapphire show that annealing induces losses of several dB/cm[116] which might be related to the relaxation at high temperature of the residual stresses through the formation of micro-cracks and twins.[129]

- Losses induced by surface roughness. This second type of loss is more complex to analyze in the literature. These losses depend on the mode considered and very few authors have analyzed films with similar thicknesses. In general, one should consider that highly confined modes and higher-order modes are more sensitive to surface effects. The typical optical surfaces for epitaxial substrates have an arithmetic roughness (RA) or root mean square roughness (RMS) better than 0.3 nm. This should give losses less than 1 dB/cm.[277] However, the growth of thin films can modify the roughness of the substrate at the interface (in-diffusion, oxidation, undulations due to stresses) and film surface roughness. The majority of publications report losses at a visible wavelength (633 nm) using a prism coupling technique. At higher wavelengths such as 1.55 μm used in the telecoms industry, the absorption and the effect of the surface roughness are less important.

Ti-indiffusion, APE or implantation guides are mature technologies for telecoms applications. The guides have low losses (0.1 dB/cm, Table 5) and can be produced with a depth of several microns.[57] LN and LT thin films with thicknesses smaller than 1 μm could provide the desired properties for developing waveguides between visible and ultraviolet wavelengths. However, to understand the potential market for such optical films, original properties/devices need to be invented. Doping of films with luminescent ions (Er, Eu, Nd), transition metal implantation or doping which affects the dispersion of wavelengths may present some interesting developments. Indeed, the massive integration of optical circuits isn't just physically limited by the optical wavelengths used but also by the limited need for integrated platforms of thousands of optical components.[278]

To summarize, the growth of thin films for photonic application made by both physical and chemical methods offers new opportunities for abrupt index profiles on different substrates, luminescence doped films,[213] damage resistant guides, complex heterostructures or superlattices.[198,279,280] Moreover, epitaxial thin films could also offer more robust processing strength. Finally, the engineering of residual stresses resulting from the substrate clamping effect and chemical engineering (doping, solid solutions, nonstoichiometry, concentration gradients) can be used for tuning or stabilizing of optical properties.

3.3. ACOUSTIC PROPERTIES AND DEVICES

Despite the high interest in LN and LT films for acoustic applications such as SAW and BAW filters and sensors, the acoustic performance of grown LN and LT films has only been reported by several groups. For this purpose, acoustic wave devices based on the Y-, Z- and 33°Y- oriented LN and LT films grown on sapphire, $LiTaO_3$, $LiNbO_3$, and Si substrates were studied experimentally. The acoustic performance (propagation velocities, electromechanical coupling, thermal coefficient of frequency (TCF)) was simulated for X-, Y-, Z- and 33°Y-oriented LN/LT films on different cuts of sapphire substrates by several groups and is summarized in **Table 6.**[101,136,138,208,281] The propagation velocities of Rayleigh waves in single crystals of LN and LT are 3400-4000 m/s and 3147-3329 m/s, respectively. As discussed above, the grown film thickness is usually limited to 500 nm due to film cracking at high thermal stresses. Thus, the simulated propagation velocities and electromechanical coupling factors at h/λ =0.1 and h/λ =0.3 (where h is LN/LT film thickness and λ – SAW wavelength), representing SAW devices with wavelength of 1.4 μm (standard SAW wavelength in filters industry) on 140 nm and 420 nm thick LN/LT films, were extracted from the literature. When an LN or LT film is grown on a sapphire substrate, which has a much higher propagation velocity (5555 m/s), a guided SAW with accelerated propagation is created. One can note that this increase in propagation velocity occurs for all orientations of LN and LT and all cuts of sapphire substrates (Table 6). For example, at h/λ =0.1, the propagation velocity is in the range of 5000-6200 m/s and is dependent on the film and substrate orientation, as well as the excited mode type and its propagation direction. The highest velocity can be obtained for the Leaky Love wave while propagating along the X-axis in a Y-LN/R-sapphire heterostructure.[208] The SAW velocities decrease with the increase in thickness of the LN/LT layers, as the wave penetration in the sapphire substrate diminishes. High-electromechanical coupling factors, K^2, can be attained in the X-, Y- and 33°Y-oriented LN films on sapphire (7-10% at h/λ =0.1 and around 22% h/λ =0.3, **Table 6**). These orientations are very promising for the design of RF SAW filters with an ultra-wide passband at a high-frequency (at 3.5 GHz). These 400 nm thick films have electromechanical coupling factors of around 20% and a phase velocity of around 5000 m/s. The integration of LN films into SAW devices would not only provide increased velocities of the AW but also it presents a possibility to find a geometry which eliminates the SAW known as the "leaky SAW" which has large losses with a YX- cut semi-infinite (thick) substrate of sapphire.[208] SAWs in 33°Y-LT/R-sapphire have slightly lower propagation velocity and the K^2 is smaller by a factor of two compared to equivalent SAWs in 33°Y-LN/R-sapphire (Table 6).[208] The K^2 is reduced at low thicknesses because of a significant contribution from the non-piezoelectric substrate. Moreover, the sapphire has a much lower TCF than that of LN and the TCF of LN films on sapphire (-50 to -80 ppm/°C)[98,281] is reduced with respect to the TCF of bulk LN (-71 to -80 ppm/°C). Therefore, a compromise should be made between a high/low velocity and a low/high K^2 when determining the required layer thickness for SAW devices based on thin films. Higher propagation velocities can be achieved by using higher order modes, which appear at $h/\lambda > 0.6$-0.7 (Table 6).[281] However, the electromechanical coupling decreases significantly with the increase of the order. To exploit these modes, the film thickness should be at least 500 nm if deep-UV lithography is used for the fabrication of these SAW devices. Overall, the key parameter defining the performance of SAWs in a material is their propagation direction. The comparison of properties of SAWs propagating along the X-axis and Z-axis projection in the surface plane ($(01\bar{1}4)$ direction) in 33°Y-LN/R-sapphire and along the X- and Y-axis in Z-LN/C-sapphire is given in the Table 6. In the case of 33°Y-LN/R-sapphire, the SAW is highly electromechanically coupled when propagating along the X-axis while K^2 decreases drastically along the Z-axis projection. In general, Z-axis oriented films are characterized by relatively low K^2. It was shown that epitaxial films have much lower insertion losses than textured films[94] and that the co-existence of several crystallographic orientations in epitaxial films may eliminate any electromechanical coupling.[208]

The experimentally measured propagation velocities, K^2, and insertion losses of SAW devices based on LN or LT films on sapphire substrates are summarized in Table 6. SAW structures were characterized on 33°Y-Z oriented LT (in this notation Z stands for the

propagation direction) and Y-X oriented LN on R-sapphire, and Z-X and Z-Y oriented LN on C-sapphire.[101,138,208,282] It is worth noting that the h/ λ ratio of the experimental devices was very small because of the fact that only the films with small thicknesses were available and the microfabricated interdigital transducers used wavelengths around 3 - 12 μm. All the published literature on SAW devices based on LN/LT films on sapphire substrates reported significantly increased propagation velocities in good agreement with simulations (Table 6). Most of the papers detailing the SAW properties of LN/LT films reported only theoretical values for the electromechanical coupling factor. Shibata et al. reported that the K^2 of 33°Y-Z oriented LT was 0.25%, which was in a perfect agreement with the simulation.[101] Last but not the least, the insertion losses were extremely high (8-50 dB) in the case of all reported SAW devices based on LN/LT films. Such high losses are not acceptable for producing an acoustic device. The experimental demonstrations of SAW devices using LN films on Si substrates indicated the poor quality of the acoustic signal as well (Table 6).[90,236] It is difficult to identify the origins of such poor quality SAW responses in the past, but it is expected to be related to the inability to control the film surface quality, nonstoichiometry/parasitic phases, twinning/nano-cracking, oxygen deficiency, and/or the quality of the microfabricated SAW devices. The frequency response of a single-port resonator with wavelength of 1 μm, fabricated on the nearly stoichiometric, smooth, twin-free Z-Y LN film with a thickness of 140 nm on C-sapphire (grown by MOCVD) is presented in the **Figure 18**. The resonator has a resonance at 4.78 GHz, low insertion losses (1 dB), K^2 of 0.9%, and relatively high quality factor (248). The propagation velocity (4780 m/s) is slightly lower than the theoretically expected one (5200 m/s). This difference probably can be explained by the fact that the LN layer was under 1.3 GPa of tensile residual stress, which modifies the density and the elastic constants of the layer.
In 1995, Nakahata et al. have reported the possibility to increase by several times the acoustic velocity in ZnO, LN and LT layers by using diamond substrates, producing the highest reported acoustic velocity.[283] The 1st order SAW mode in a Z-LN/diamond heterostructure with h/ λ=0.08 had an acoustic velocity up to 12 000 m/s and K^2 of 9% (Table 6). Moreover, such diamond based structures have very low propagation losses. This initial work provided the basis for further research on ZnO and LN films on diamond based substrates. Very high propagation velocities (8200 -14900 m/s) were measured experimentally in SAW devices based on LN films and poly-diamond. The studied LN films had a range in texture quality, starting from a polycrystalline state[284] to films with preferential (0001)[200,285] or $(11\bar{2}0)$[286] textures. The highest velocities were measured in the c-axis textured LN films on diamond.[200,285] The insertion losses were very high and probably were related to the polycrystallinity of the LN films and their high roughness (Table 6).[284] In this case the LN layer texture and surface quality were not sufficient for the production of high frequency SAW devices.

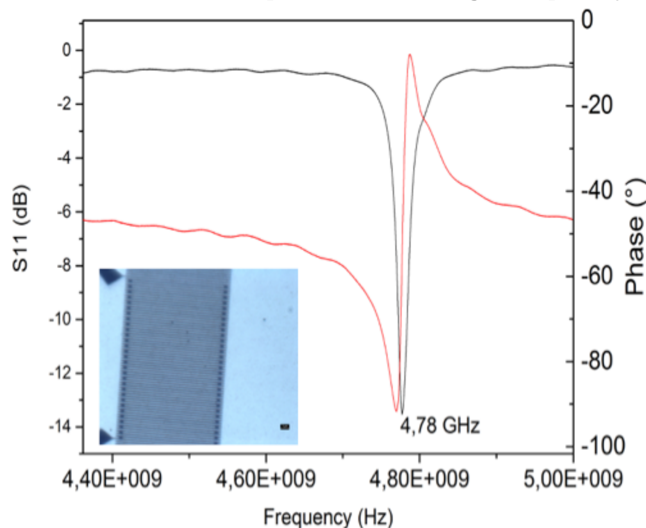

Figure 18. Frequency response (S_{11} and phase) of a single-port resonator with a wavelength of 1 μm based on a nearly-stoichiometric 150 nm thick C-$LiNbO_3$ film grown by pulsed injection MOCVD on C-sapphire. The optical image of the 50 nm thick Al interdigital electrodes with a period of 500 nm is given

in the inset.

A significant advance in AW devices based on LN films was reported by Kadota and collaborators. They microfabricated a structure consisting of epitaxial Z-LN films/(electrode)/air gap/substrate, which was adapted for utilising the Lamb waves[188,189,250] and TFAR devices[83] (**Figure 19** and **20**). First, ZnO was deposited on an LN substrate and structured by lithography. Then, Z-LN layers were deposited on the ZnO/LN by CVD and the ZnO was then etched by dry or wet etching to liberate the membrane. Following the etching the top electrodes are deposited. Using this fabrication method one port Lamb resonators operating at 4.5 GHz and 6.3 GHz (very high velocities of 12500 m/s and 14 000 m/s) with large impedance ratios at resonance and anti-resonance frequencies, and wide bandwidth (7.2% and 3.7%) was demonstrated (Figure 19).[250] The frequency response was free of parasitic modes.[250] The same approach was used to fabricate a TFBAR with a resonance frequency of 2.9 GHz based on Z-LN films(Figure 20).[83] However, it was concluded that other orientations of LN with higher K^2 would be preferable for TFBAR devices. In both devices the quality factors were not high enough and the K^2 was lower than the theoretically expected ones because of the ferroelectric polydomain structure of the films.[83,250]

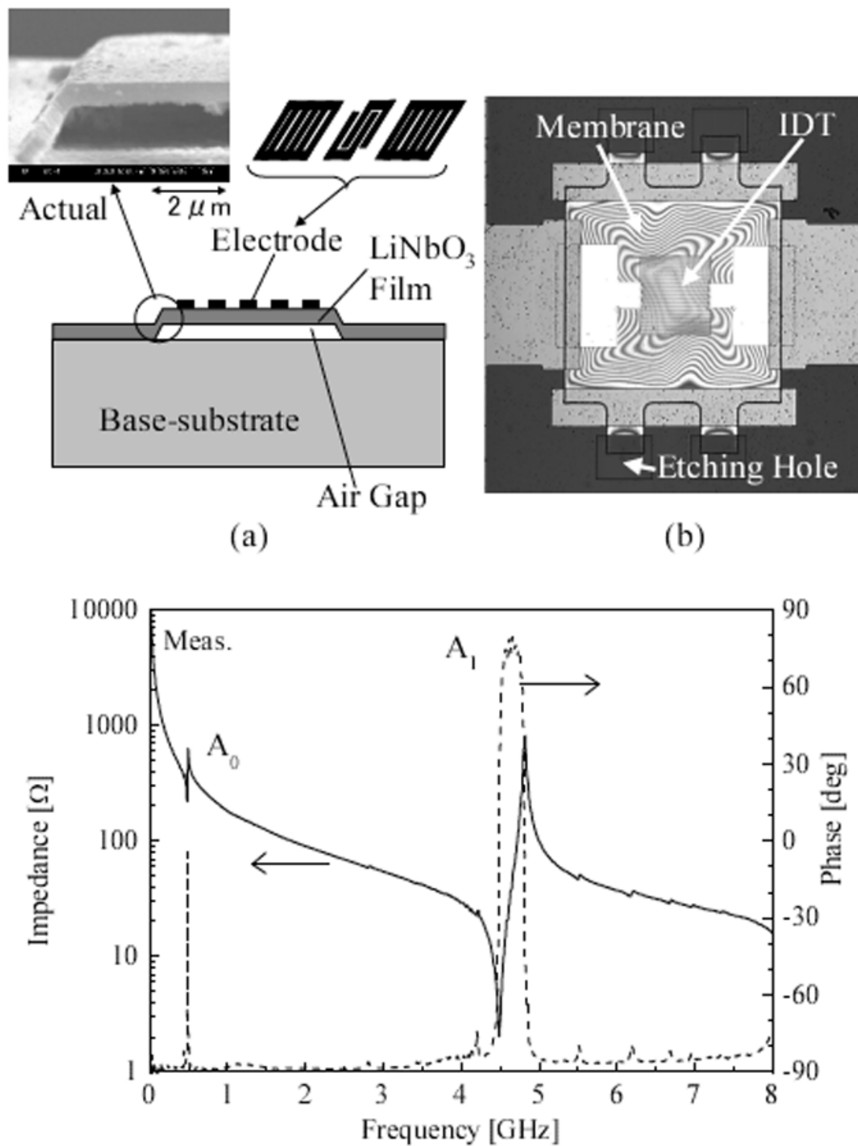

Figure 19. A high frequency one –port Lamb wave resonator fabricated from a $LiNbO_3/ZnO/LiNbO_3$ heterostructure (layers grown by CVD) with a schematic representation of the cross sectional structure in (a), the top-down optical image of the device in (b), and the measured impedance and phase as a function

of frequency (right image) in (c).
Reproduced with permission. [250] Copyright 2009, IEEE.

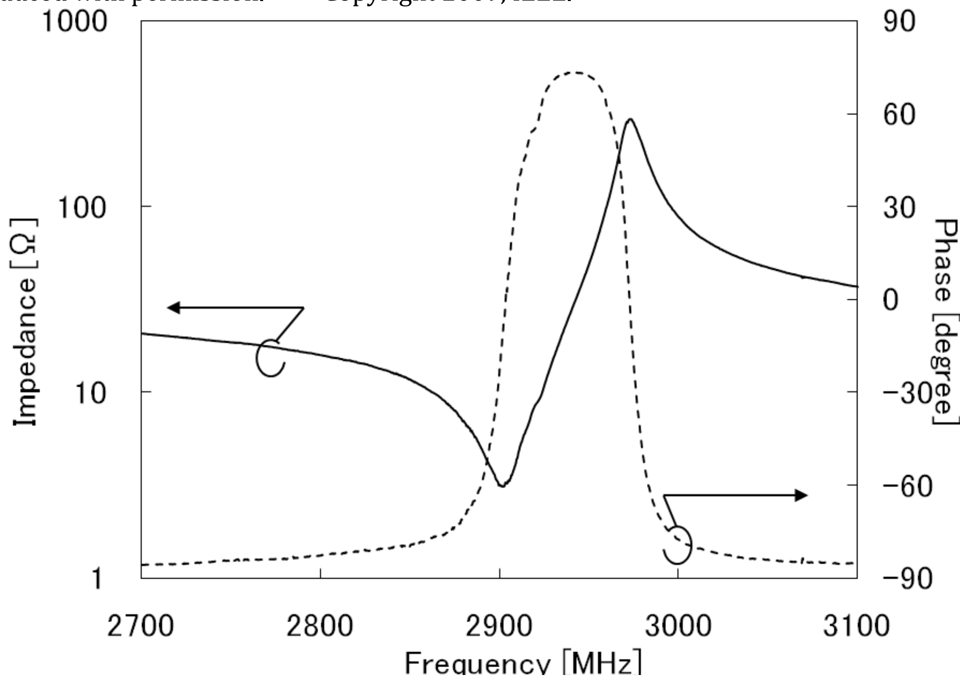

Figure 20. Measured impedance and phase as a function of frequency of an FBAR resonator fabricated from a $LiNbO_3/ZnO/LiNbO_3$ heterostructure (layers grown by CVD).
Reproduced with permission. [83] Copyright 2010, IEEE.

3.4. FERROELECTRONIC DEVICES

The integration of LN and LT films into ferroelectronic devices opens up the possibility for a number of multifunctional devices combining the piezoelectric, acoustic, pyroelectric, ferroelectric or semiconducting properties at micro and nano-scales. So far, ferroelectric memories,[187,287,288], pyroelectric devices,[97,289,290] field transistors,[291] short wavelength pockels effect based opto-electronics[187] utilising LN/LT have been studied. The use of epitaxial layers offers the opportunity for photonic and electronic integrated circuits. Several attempts have been made towards the integration of LN or LT with silicon (CMOS) structures,[292] oxide Nd:$SrTiO_3$ substrates,[63,202] III-V semiconductors[192,197] and II-VI ZnO semiconductors.[97,288,290] For example, the heterojunction of LN/ZnO/n-Si had a good photoresponse and the electrical properties of this heterojunction could be tuned by changing the composition or thickness of the layers (**Figure 21**).[229] This type of heterostructure is also compatible with acoustic wave devices and nanophotonics. The bandgap and Fermi level are integral to the performance of electronic devices. For $LiNbO_3$ and $LiTaO_3$ N-type semiconducting properties were obtained using reducing treatments[272,293] and by doping crystals with Fe or Cu.[287] While P-type semiconductor properties of $LiNbO_3$ and $LiTaO_3$ were measured in Li deficient LN films grown by PLD[202] or with Zr^{4+} or Hf^{4+} ion doping.[294] Innovative ferroelectronic designs can be made by utilising and studying the charged domain walls or current leakages.[295] Graded ferroelectric structures[296] and superlattices with enhanced properties[289] can be fabricated by the versatile MOCVD technique, enabling fine control of the precursor feeding rates.

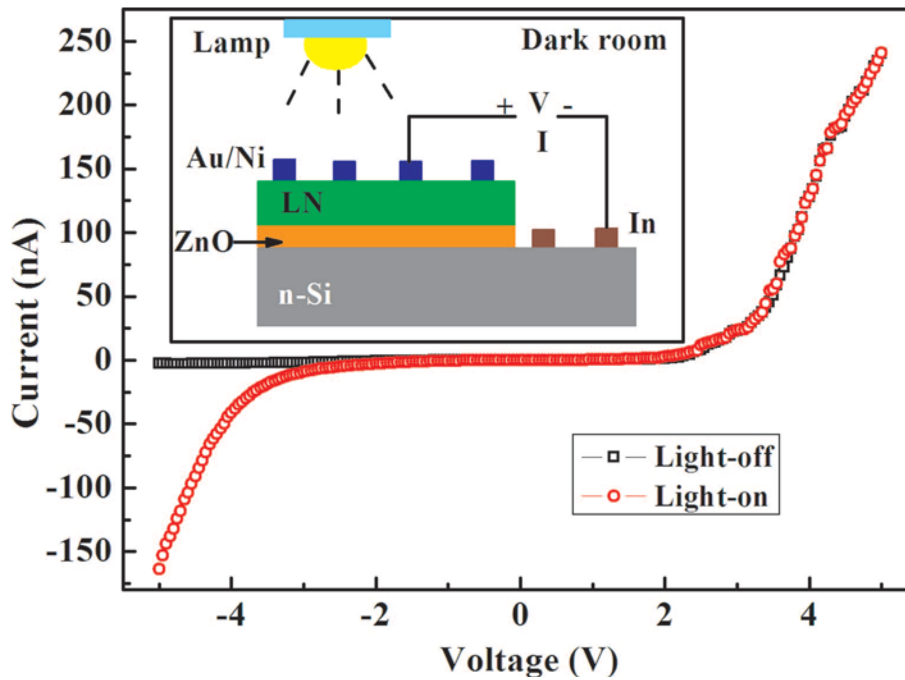

Figure 21. I-V curves of a $LiNbO_3$/ZnO/n-Si heterojunction (schematically represented in the inset) in dark and light conditions.
Reproduced with permission. [229] Copyright 2013, AIP.

4. Final remarks and outlook

Considerable effort has been done in order to optimise the textured and epitaxial growth of c-axis oriented LN/LT films on single crystalline substrates and Si. These films are of particular interest for their optical and pyroelectric applications. However, this orientation has high in-plane thermal expansion and a low elastic limit. Thus, the growth of thick C-LN/LT films is very challenging because of crack and twin formation. The electrical poling of c-axis oriented films grown on dielectric substrates is very difficult, as well. In addition to these growth difficulties the Li nonstoichiometry in most of the studied films was unknown and/or not optimised. These problems resulted in the physical properties of the resultant polydomain, twinned and highly nonstoichiometric LN/LT films not being comparable to those of single crystals and grown LN/LT films receiving a "bad reputation". Recent results indicated that the Li nonstoichiometry can be precisely controlled in thin films and that high quality acoustic performance can be achieved in LN films grown by CVD techniques. MOCVD seems to be the most promising technique for the growth of high quality alkaline niobate and tantalate epitaxial films at industrial scale because of the fine control of the Li composition and film thickness allowed with this technique. Physical methods using high-vacuum growth conditions induce significant Li_2O loss and are also limited by the Li species not being distributed homogeneously in the plasma. These affect the up-scaling of the LN/LT growth to large surfaces. Additional effort has to be made in order to optimise the quality and properties of X-, Y- and 33°Y-oriented LN/LT films, which offer higher electromechanical coupling possibilities than Z-LN/LT, and to design the acoustic, piezoelectric and optical devices based on these orientations. Furthermore, the elastic limit of X- and Y- oriented films are higher resulting in a reduction in the cracking and twinning in these orientations. The integration of orientations with oblique or in-plane orientations of the polarization axis with silicon technology has to be considered. Electrical poling and microstructuring techniques, adapted the LN/LT thin films, also have to be optimised in parallel, as well. The impact of LN/LT films on the performance of the acoustic/ piezoelectric, electro-optical, pyroelectric and ferroelectronic devices and the opportunities for applications and multifunctional integrated devices are summarized in the **Figure 22**.

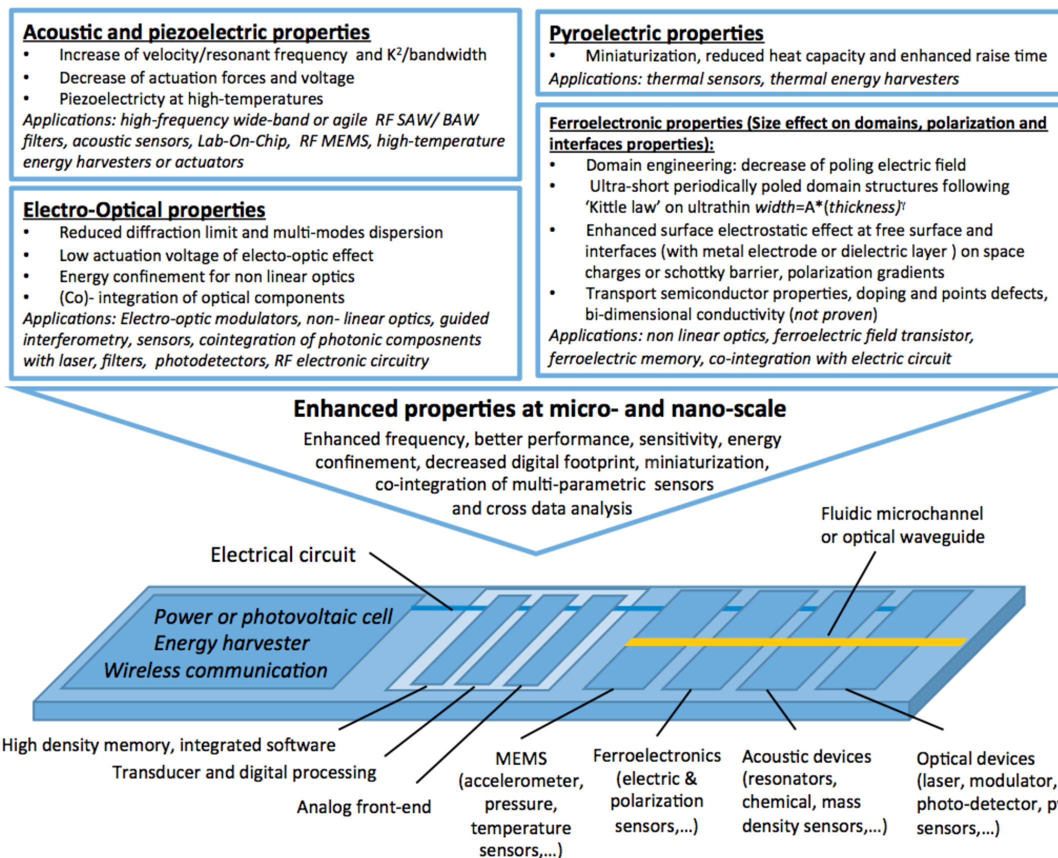

Figure 22. Application possibilities of the $LiNbO_3$ and $LiTaO_3$ films. Impact of the integration of these films on the performance of the acoustic/ piezoelectric, electro-optical, pyroelectric and ferroelectronic devices and opportunities for multifunctional co-integrated devices.

The next generation of high – frequency (5-6 GHz) and/or wide-band RF filters or frequency-agile filters are urgently needed for the development of 5th generation (5G) of infrastructures/networks/communications. In 2017, Murata Manufacturing starts mass production of a high performance SAW duplexer, based on an energy confined structure including single-crystalline LT films.[297] The acoustic wave energy was confined in the LT layer by using a multi-layered structure of low and high impedance layers on Si. These SAW resonators have a three times larger Q-factor, an 80 % reduced TCF and a 12% wider bandwidth in comparison to conventional SAW resonators based on LN/LT single crystals. The low insertion loss, high attenuation and good thermal stability achieved in these filters would allow their use in a broader frequency range. However, the fabrication of the films from single-crystals is not time-, energy- and cost-efficient. The integration of wafer-bonded films on 3D structures is challenging, as well. The introduction of the technology, based on the epitaxial/textured growth of highly coupled LN/LT films on single crystalline wafers or the standard structured Si wafers could be a real breakthrough in the RF and communication industry. Thin films of LN would devices to profit from the high K^2/wide bandwidth and to attain high frequencies with the increased propagation velocity and reduced thickness of the piezoelectric layer in SAW and BAW filters. It would allow the telecommunication frequencies to be increased from 2-3 GHz to 6 GHz and a doubling of the bandwidth. This is of special interest for 5G communication networks, will operate in a frequency range up to 6 GHz and require increasing data transfer rates by 100 times without increasing the system size. It would also open new opportunities for the development of frequency-agile filters and reconfigurable RF front-ends. This would radically reduce the number of components and increase the communication efficiency (faster speed, more information and improved functionalities in smartphones). Integration of LN films on Si would allow further miniaturization of filters by integration of devices on the same Si chip. Moreover, $LiNbO_3$[298] (LN) presents a figure of merit in vibrational energy harvesting similar to that of PZT.[299] LN is compatible with high-temperature

applications of transducers (up to 1000 °C)[300] and energy harvesters (at least up to 500 °C, further experiments are needed to find the temperature limit).[301] This makes LN particularly attractive for energy scavenging applications where the working temperature is elevated (in oil, exhaust pipe, close to motors where the temperature can reach 600 °C), as PZT, $BaTiO_3$ and $K_{1-x}Na_xNbO_3$ loss their piezoelectric properties at these temperatures. Although, the pyroelectric properties of LN and LT were not discussed in this paper, it is important to note that LT single crystals are used for the industrial fabrication of pyroelectric sensors. Thus, c-axis textured/epitaxial LT thin films are of particular interest for the miniaturized and integrated pyroelectric sensors with a reduced heat capacity and enhanced rise time. LT films can be considered for thermal energy harvesting because of their high pyroelectric coefficient and relatively high Curie temperature (600 - 700 °C). As described above, LN is one of the most important crystals, in the fields of photonics, optics, nonlinear optics and optoelectronics. Therefore, beyond the applications in RF filters and sensors, thin film technology adapted for the Z- or X-LN films on substrates with big difference in refractive index may have numerous applications in integrated optics and opto-acoustic devices that couple wirelessly to optical fiber networks. In this field, thin films can offer better energy confinement, low-power devices, modulators with large bandwidths, reduced diffraction limits and new functionalities in nanostructured surfaces. LN films are also attracting the attention of the rapidly emerging field of ferroelectronics for their high spontaneous polarization (71 μC/cm^2). However, in LN films further detailed studies of the effects of size on the domains, polarization, interface and surface properties are required. To summarize, LN and LT epitaxial films need to be developed in order to contribute to the race towards 5G applications and high frequency communication technologies. The CMOS-compatible integration of LN/LT films on Si could open new possibilities of the integration of MEMS, ferroelectronic, acoustic and optical devices, etc. on the same chip (Figure 22).

Table 1. Conventional labelling of cuts of rhombohedral and hexagonal materials (LN, LT, sapphire, $LaAlO_3$, ZnO, AlN, GaN) in the orthogonal XYZ setting, hexagonal setting, IEEE convention and the Euler angles.

Cut	Plane	Axis	IEEE convention	Euler angles
X	$(2\bar{1}\bar{1}0)$ A-plane	$[2\bar{1}\bar{1}0]$ a-axis	90°/90°(YXlt) or XY plate	(0,90,0)
Y	$(01\bar{1}0)$ M-plane	$[01\bar{1}0]$	YX plate	(90,90,0)
Z	$(01\bar{1}0)$ C-plane	[0001] c-axis	90°(YXl)or ZX plate	(0,0,0)
33°Y	$(01\bar{1}2)$ R-plane		33°(YXl)	(0,122°23’,0)

Table 2. Comparison of sublimation, T_{Subl}, decomposition, T_{Dec}, evaporation, T_{Evap}, and deposition, T_{Dep}, temperatures, and Li/Nb or Li/Ta ratios used to grow single-phase LN or LT films, respectively. The solubility and the stability are given, as well. (O^tBu = tert-butoxide, thd = 2,2,6,6-tetramethyl-3,5-heptadionate, OEt = ethoxide, OMe = methoxide, acac = acethylacetonate, dmae – dimethylaminoethanol)

Compound (state at RT)	T_{Subl}, °C	T_{Dec}, °C (residue %)	T_{Evap}, °C	T_{Dep}, °C	Ratio Li/Nb (Li/Ta)	Solubility and stability
			Depositions using $Li(O^tBu)$			
[$Li(O^tBu)]_6$ (solid)	>170-205	>250[175]	108[302] 115[303]			Toluene, hexane, THF, MTBE Stable at RT, air and moisture
$Nb(OEt)_4$(dmae) [302]			79.5	650	1.65 - 3.4	
[$Nb(OEt)_5]_2$ (liquid)		>325-350	135[303] 130[175]	450-630[303] 650[175]	2.3[175]	Dry toluene, ethanol Reacts with moisture
			Depositions using Li(thd)			
Li(thd) (solid)	270[304] < 400[118]	295-330 (15%)[304] RT[175]	200[117,118,305] 250[115] 280[306]			Water, ethanol Insoluble in toluene Air and moisture stable
$Nb(thd)_4$ (solid)		325 (16.1%) [174] RT[175]		600-650 [129, 174] 500-750[116]	3.25-3.75[174] 4.0 [174] 1.25[129] 1.86[116]	1,2-dimethoxyethane Insoluble in water Air and moisture stable
$Nb(thd)_2Cl_3$ (solid)			170[305]	600-750[305]	2.85[305]	
$Nb(OMe)_5$			200[115]	450[115]		
$Nb(OEt)_5$ (liquid)		>325-350	135-145[117] 100-120[118]	600-700[117] 650-750[118]	1.06-1.76[118]	Dry toluene, ethanol Reacts with moisture
$Ta(OEt)_5$ (liquid)		>275[307]	120[308]	600[173,240]		Organic solvents, water
$Ta(OEt)_4$(acac) (solid)			210-250	700[146]		1,2-dimethoxyethane
			Depositions using Li(acac)			
Li(acac) & $Ta(OEt)_5$[173]			aerosol	550-650	0.7	Methanol
			Bimetallic precursors			
$LiNb(OEt)_6$[176]	disproportionates to $Nb(OEt)_5$[309]		270-340[306]	490-590[306]		
$LiTa(OEt)_6$ [176]			280[177]	425-572[177]		
$LiNb(OBu)_6$	110-120 [309] 100-200 [120]					
$LiTa(OBu)_6$ (solid)	110-120 [309] 100-200 [120]	300-400 [120]		550-800[120] 550-780[82] 750[122,172]		

Table 3. In-plane lattice parameters, in Å, of Z-, 33°Y-, Y- and X-oriented LN/LT and the rhombohedral, hexagonal and cubic substrates, used for the epitaxial growth of LN/LT films. Note that the planes matching epitaxially are arranged in one column. (01$\bar{1}$4)' – plane (01$\bar{1}$4) is tilted by 5 ° from the surface plane.

LN & LT growth orientation	Z (0001)		33°Y-X (01$\bar{1}$2)		Y (10$\bar{1}$0)		X (11$\bar{2}$0)	
⊥ surface	(11$\bar{2}$0)	(30$\bar{3}$0)	(11$\bar{2}$0)	(01$\bar{1}$4)'	(11$\bar{2}$0)	(0006)	(30$\bar{3}$0)	(0006)
$LiNbO_3$ (R3c) [310]	2.576	1.487	2.576	2.736	2.576	2.310	1.487	2.310
$LiTaO_3$ (R3c) [311]	2.574	1.486	2.574	2.724	2.574	2.294	1.486	2.294
Rhombohedral substrates								
//surface	(0001)		(01$\bar{1}$2)		(10$\bar{1}$0)		(11-20)	
⊥ surface	(11$\bar{2}$0)	(30$\bar{3}$0)	(11$\bar{2}$0)	(01$\bar{1}$4)'	(11$\bar{2}$0)	(0006)	(30$\bar{3}$0)	(0006)
Sapph. (R$\bar{3}$c) [312]	2.380	1.374	2.380	2.551	2.380	2.166	1.374	2.166
$LaAlO_3$(R$\bar{3}$c) [313]	2.683	1.549	2.683	2.679	2.683	2.185	1.549	2.185
Hexagonal substrates and buffer layers								
//surface	(0001)		(11$\bar{2}$0)		(10$\bar{1}$0)			
⊥ surface	(10$\bar{1}$0)	(11$\bar{2}$0)	(0002)	(10$\bar{1}$0)	(0002)	(11$\bar{2}$0)		
AlN (P63mc) [314]	2.695	1.556	2.490	2.695	2.490	1.556		
GaN (P63mc) [315]	2.762	1.595	2.593	2.762	2.593	1.595		
ZnO (P63mc) [316]	2.812	1.623[207]	2.602	2.812[316]	2.602	1.623[209]		
Cubic substrates and buffer layers								
//surface	(111)		(100)					
⊥ surface	(1$\bar{1}$0)	(11$\bar{2}$)	(011)	(01$\bar{1}$)				
LSAT (Pn3m)	2.735	1.579	2.735 a)	2.735 a)				
$SrTiO_3$(Pm$\bar{3}$m) [317]	2.761	1.594	2.761	2.761				
Pt (Fm$\bar{3}$m) [318]	2.774 a)	1.387 a)	2.774	2.774				
Y_2O_3 (Ia$\bar{3}$) [319]	7.460	4.308						
⊥ surface	(22$\bar{4}$)	(2$\bar{2}$0)						
MgO (Fm$\bar{3}$m)	0.860	1.489	2.978	2.978				
⊥ surface			(002)	(020)				
GaAs (F$\bar{4}$3m)	1.154	1.999	2.827	2.827				
Si (Fd3m)	1.109	1.920	2.715	2.715				
Y_2O_3 (Ia$\bar{3}$) [319]			2.638(/2)	2.638(/2)				
Other substrates								
//surface	(100)		(110)					
⊥ surface	(020)	(002)	(1$\bar{1}\bar{2}$)	(1$\bar{1}$2)				
$NdGaO_3$ (Pbnm)			2.729	2.729				
YSZ (Fm$\bar{3}$m)	2.570 a)	2.570 a)						

a) Unpublished work.

Table 4. Thermal expansion along different directions (at 300 K) of $LiNbO_3$, $LiTaO_3$, buffer layers and substrates. Note that in hexagonal and rhombohedral crystal systems the thermal expansions along the X- and Y-axis are equal and the cubic system has isotropic thermal expansion. The values were multiplied by *10^6 and given in °C^{-1}.

Rhombohedral materials (hexagonal settings)			
Planes	$(11\bar{2}0)$	(0006)	$(01\bar{1}4)$'
$LiNbO_3$[146]	19.2	2.7	7.6
$LiTaO_3$ [146]	19.1	-0.9	5.0
Sapphire[320]	4.5	5.3	5.1
$LaAlO_3$[321]	10	-	-
Hexagonal materials			
Planes	$(11\bar{2}0)$	(0002)	
AlN[322]	4.3	3.5	
GaN [322]	3.4	3.3	
ZnO [322]	4.3	2.5	
Cubic materials			
LSAT[323]	8.2	Si	2.6
$SrTiO_3$[324]	9	GaAs	6.5
Pt	9	YSZ[325]	9
MgO[326]	14.0	Y_2O_3[327]	8.1
Orthorhombic	$NdGaO_3$[328]	9	

Table 5. Refractive indices (n_o and n_e are the ordinary and extraordinary indices, respectively), electro-optic coefficients (r_{33} and r_{31}) and propagation losses of waveguides fabricated from LN and LT single crystals and thin films by different methods. TE and TM stand for transverse electric and transverse magnetic, respectively.

Refractive index (λ=633 nm)		Propagation losses (λ=633 nm)	Electro-optic (λ=633 nm)	Remarks
$LiNbO_3$				
n_o	n_e			
2.29	2.19 to 2.22 +0.03[28]			Effect of Li nonstoichiometry in crystals Change from 50 to 46.1 mol% of Li[20]
		<0.008 dB/cm (λ =514 nm)		Crystal annealed in O_2 and poled[273]
		<0.1 dB/cm[274]	r_{33}=31 pm/V[329] r_{13}=11 pm/V	Limited by damage and photorefractive effect
+0.02 TE	+0.03 TM	<0.3 dB/cm		Ti diffused guide[57,274]
-0.04	+0.12 TM	0.5-1 dB/cm		Proton exchanged guide[40,57,330]
		0.5 dB/cm		F swift heavy-ion irradiation[331]
-0.02 TE	-0.01 TM	0.5-1 dB/cm		H^+, He^+ implantation [330,332]
$LiNbO_3$ films				
2.27	2.19		r_{33}=31 pm/V r_{13}=11 pm/V	Smart Cut (values equivalent to bulk) [51]
~2.29	<2.19	1 dB/cm		LPE-grown layer on MgO:LN substrate [260]
2.26-2.27	2.18-2.19	1 to 6 dB/cm		MOCVD, film on (0001)-sapphire[135,333] Effect of annealing, roughness, stress,..
		6 to 40 dB/cm		CVD on LT, [115,334] not guiding films
2.26	2.21			PLD, film on (0001)-sapphire[161]
		1.5 dB/cm		PLD, film on (0001)-sapphire[95]
		2 to 4 dB/cm		PLD, film on ZnO/(0001)-sapphire[335] Residual conductivity of ZnO
2.263	2.199			Sputtering, film on SiO_2/Si[235]
			r_{33}=23.2 pm/V	Stacked layer/substrate structure: TiN/LN/Si,[336] ZnO/LN/ZnO[187]
			r_{33}=18 pm/V	Sputtering TiN/SiO_2/LN/Si[337]
2.28	2.19	0.5 dB		Sol-gel, film on CLN[91]
2.1 (amorphization)		< 0.5 dB/cm		Fluorine ions implantation[338]
2.1 (amorphous) 2.25 (polycrystalline)		3 dB/cm 20 dB/cm		RF-sputtering, glass and crystalline substrates, before and after annealing [60]
		Li conductivity		(amorphous) RF-magnetron on ITO-coated glass substrates[275]
$LiTaO_3$				
2.177	2.181			Poled crystals[339]
		<0.005 dB/cm (λ =514 nm)		Annealed in O_2 and poled crystal[273]
			r_{33}=30.5 pm/V r_{13}=8.4 pm/V	Poled crystals[340]
$LiTaO_3$ films				
Composition dependent		>20 dB/cm 0.8 dB/cm (λ = 1.15 µm)		LPE, $LiNb_{1-x}Ta_xO_3$/LN[341]
2.163	2.177			PLD, film on (0001)sapphire[100]
		5.9 dB (as grown) 2 dB (annealed)	r_{33}=1 pm/V (as grown) r_{33}=12 pm/V (poled films)	MOCVD, film on $(11\bar{2}0)$ sapphire[172]
1.84				Sol-gel, film on SiO_2/Si, index lower than that of bulk due to crystallinity and micropores[342]

Table 6. Simulated and experimentally measured propagation velocities, v, electromechanical coupling factor, K^2, and insertion losses (losses) of SAW devices based on deposited LN and LT films. h is the film thickness and λ the SAW wavelength. The diamond layers and substrates were polycrystalline. The propagation velocities of Rayleigh waves in single crystals of sapphire, LN and LT are 5555 m/s, 3400-4000 m/s, and 3147-3329 m/s, respectively.

		Simulations			Experimental data			
Heterostructure	Order/ wave	h/ λ	v, m/s	K^2,%	h/ λ	V, m/s	K^2,%	Losses, dB
(90°, 90°, 0°), YX orientation, propagation along X								
LN/M-sapphire[281]	1st	0.1	5800	7				
		0.3	5100	22				
	2nd	0.6	5900	7				
	3rd	0.7	5800	3				
LN/R-sapphire	1st [281]	0.1	6200	7	0.2[208] a)	5194		8.5
		0.3	5250	22				
	Leaky Love[208]	0.1	6200	10				
	Love	0.3	5200	23				
(0°, 90°, 0°), XZ orientation								
LN/A-sapphire[281]	1st	0.1	5800	10				
		0.3	5200	19				
	2nd	0.6	5700	3.5				
	3rd	0.7	5700	2.5				
33°YX orientation								
Propagation along X								
LT/R-sapphire[208]		0.1	5650	5.5				
		0.3	4700	10				
LN/R-sapphire[208]		0.1	6100	10				
		0.3	5150	21.5				
Propagation along Z-axis projection								
LT/R-sapphire	Rayleigh	0.1[101]	5000	0.4	0.022 [138], b)	5700		20
		0.3[138]	4000	0.2	0.023 [138], b)	5700		9
	Sezawa	0.3[138]	5800	4.5	0.04[101]	5400	0.25	20
ZX orientation								
Propagation along X								
LN/C-sapphire	Rayleigh[208]	0.1	5200		0.025 [282], c)	5997		50
		0.3	4500		0.035[101]	5416		20
	Leaky	0.1	6000	3.8	0.035[101]	6480		8
	Love	0.3	5100	6.8				
Propagation along Y								
LN/C-sapphire	Rayleigh [136]	0.1	5450		0.023 [101]	5520		46
		0.15	5200		0.14 d)	4780	0.9	1
LN/Si					0.15[90]	4500		60
LN/Y_2O_3/Si[236]							3 a), b)	3 a), b)
LN/diamond/Si	1st[283]	0.08	12000	9	0.08 [285,286]	12474	4.85 e)	
	0th	0.03	8700	<0.3	0.03[284]	8200	0.93	25
LN/Al_2O_3/diamond					0.03 [200], a)	14900		

a) Experimentally measured frequency response is not presented as a proof; b) propagation direction is not indicated; c) film without preferential orientation in the plane; d) this work; e) the quality of the frequency response was poor because of the low quality factor or/and low K^2, it cannot be used to estimate K^2.